

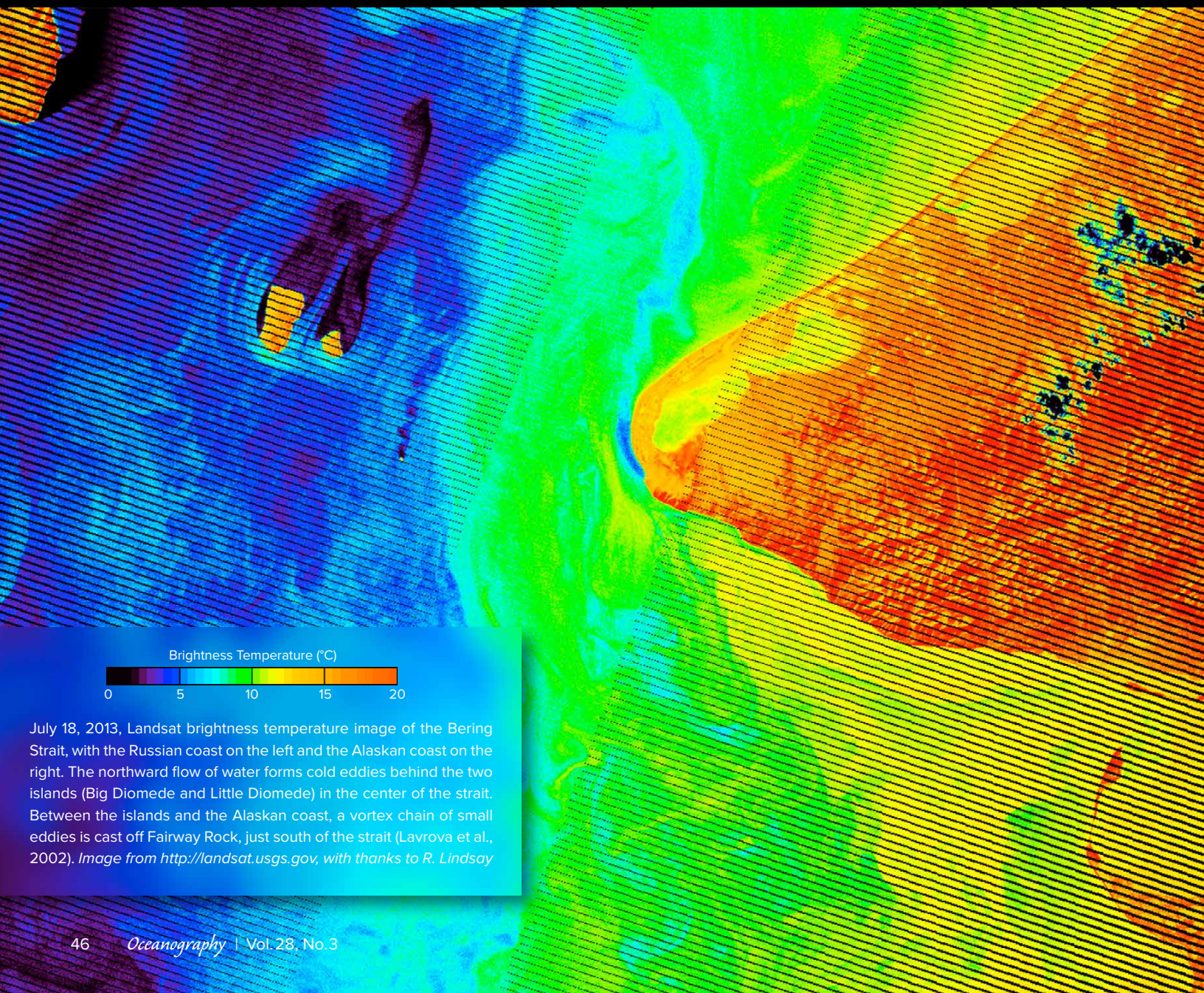
A Synthesis of Year-Round Interdisciplinary Mooring Measurements in the Bering Strait (1990-2014) and the RUSALCA Years (2004-2011)

The Faculty of Oregon State University has made this article openly available.
Please share how this access benefits you. Your story matters.

Citation	Woodgate, R. A., Stafford, K. M., & Pahl, F. G. (2015). A Synthesis of Year-round Interdisciplinary Mooring Measurements in the Bering Strait (1990-2014) and the RUSALCA years (2004-2011). <i>Oceanography</i> , 28(3), 46-67. doi:10.5670/oceanog.2015.57
DOI	10.5670/oceanog.2015.57
Publisher	Oceanography Society
Version	Version of Record
Terms of Use	http://cdss.library.oregonstate.edu/sa-termsfuse

A Synthesis of Year-Round Interdisciplinary Mooring Measurements in the Bering Strait (1990–2014) and the RUSALCA Years (2004–2011)

By Rebecca A. Woodgate, Kathleen M. Stafford, and Fredrick G. Prah



Brightness Temperature (°C)



July 18, 2013, Landsat brightness temperature image of the Bering Strait, with the Russian coast on the left and the Alaskan coast on the right. The northward flow of water forms cold eddies behind the two islands (Big Diomedes and Little Diomedes) in the center of the strait. Between the islands and the Alaskan coast, a vortex chain of small eddies is cast off Fairway Rock, just south of the strait (Lavrova et al., 2002). Image from <http://landsat.usgs.gov>, with thanks to R. Lindsay

ABSTRACT. The flow through the Bering Strait, the only Pacific-Arctic oceanic gateway, has dramatic local, regional, and global impacts. Advanced year-round moored technology quantifies challengingly large temporal (subdaily, seasonal, and interannual) and spatial variability in the ~85 km wide, two-channel strait. The typically northward flow, intensified seasonally in the ~10–20 km wide, warm, fresh, nutrient-poor Alaskan Coastal Current (ACC) in the east, is otherwise generally homogeneous in velocity throughout the strait, although with higher salinities and nutrients and lower temperatures in the west. Velocity and water properties respond rapidly (including flow reversals) to local wind, likely causing most of the strait's approximately two-layer summer structure (by "spilling" the ACC) and winter water-column homogenization. We identify island-trapped eddy zones in the central strait; changes in sea-ice properties (season mean thicknesses from <1 m to >2 m); and increases in annual mean volume, heat, and freshwater fluxes from 2001 to present (2013). Tantalizing first results from year-round bio-optics, nitrate, and ocean acidification sensors indicate significant seasonal and spatial change, possibly driven by the spring bloom. Moored acoustic recorders show large interannual variability in sub-Arctic whale occurrence, related perhaps to water property changes. Substantial daily variability demonstrates the dangers of interpreting section data and the necessity for year-round interdisciplinary time-series measurements.

WELCOME TO THE PACIFIC GATEWAY TO THE ARCTIC OCEAN

The western Arctic landmass has been home to native communities of humans for 10,000–20,000 years (Hoffecker and Elias, 2003). Deglaciation ~15,000–10,000 years ago led to a rise in sea level and the opening of the oceanic channel we now call the Bering Strait, likely stabilizing world climate (Dyke et al., 1996; Hoffecker and Elias, 2003; De Boer and Nof, 2004) and leading eventually to the development of a maritime culture in the region at least 3,500 years ago (for overview, see Fitzhugh, in press). Ever since the first explorers passed through the Bering Strait (Semyon Dezhnyov in 1648; Cossack Chief Ermak before 1650; Vitus Bering in 1728; see, e.g., Black, 2004), nations have realized the potential for this narrow channel as a gateway to Arctic riches. The western Arctic whaling boom (1848–1908) saw a dramatic increase in shipping through the strait (one ship in 1848; over 220 ships in 1852; Bockstoce, 1986), eager to exploit

the rich ecosystem just north of the strait in the Chukchi Sea. In present times, as summer Arctic sea-ice cover is dramatically decreasing (Stroeve et al., 2007, 2014), a new Arctic rush is taking place, with the Bering Strait offering the gateway for trans-Arctic shipping and access to the natural resources being revealed by the retreating ice.

Besides its role as a geographical barrier, the narrow (~85 km wide), shallow (~50 m deep) Bering Strait plays a remarkably large role in local and global climate. It is the only conduit for ocean waters between the Pacific and the Arctic Oceans. Although the flow through the strait is modest in global terms (~0.8 Sv; Roach et al., 1995; 1 Sv = 1 Sverdrup = $10^6 \text{ m}^3 \text{ s}^{-1}$) compared to the Gulf Stream (between 30–85 Sv; e.g., Pickard and Emery, 1990), the impact of the Bering Strait throughflow is substantial—locally, in the Arctic, and globally. By providing a northward exit, the flow through the strait has an important draining influence on the Bering Sea shelf to the south (Stabeno et al., 1999; Zhang et al., 2012),

a region that provides ~50% of the US fish catch (Sigler et al., 2010). North of the Bering Strait, the throughflow dominates the properties and residence time of waters in the Chukchi Sea (Woodgate et al., 2005b), which is in turn one of the most productive areas of the world ocean (Grebmeier et al., 2006a). In the Arctic proper, waters of the throughflow (often referred to in the Arctic as Pacific waters, since the Bering Strait is the sole source of Pacific water to the Arctic) are an important source of nutrients for Arctic ecosystems (Walsh et al., 1997); act as a trigger for the melt back of Arctic sea ice in summer (Woodgate et al., 2010b); and provide about one-third of the freshwater entering the Arctic (Aagaard and Carmack, 1989). The throughflow also provides a conduit for contaminants into the Arctic Ocean (Macdonald et al., 2003).

Pacific waters are found throughout roughly half the area of the upper (shallower than ~100 m) Arctic Ocean (Jones and Anderson, 1986; Steele et al., 2004), where they likely influence western Arctic sea-ice retreat in two opposing ways (Francis et al., 2005; Shimada et al., 2006; Woodgate et al., 2010b)—the summer Pacific water provides a subsurface source of heat to the sea ice in winter, and the winter Pacific water below forms a protective layer between the sea ice and the warmer Atlantic waters deeper in the Arctic water column (for a brief review of Arctic Ocean circulation, see Woodgate, 2013). The nutrients brought into the Arctic by the Pacific waters fuel Arctic ecosystems and biological productivity also in the areas where they exit the Arctic Ocean (Jones et al., 2003), especially the polynya regions of the Canadian Arctic Archipelago (e.g., Tremblay et al., 2002).

Via its contribution to Arctic freshwater outflow, the influence of the Bering Strait is also felt in the Atlantic Ocean, with implications for global

climate stability. Modeling studies (see, e.g., Wadley and Bigg, 2002, for a review) suggest the throughflow can influence the path of the Gulf Stream and the Atlantic Overturning Circulation, and paleo studies attribute modern climate stability to the balancing influence of the Bering Strait throughflow (De Boer and Nof, 2004; Hu et al., 2007).

The remarkably broad impacts of the Bering Strait throughflow drive the desire to quantify and explain its properties, both for local and global environmental and climate studies and to anticipate the impacts and challenges of economic growth in the region. In this article, we address the observational challenges of the strait and the interdisciplinary progress that has been made in recent decades, especially since the advent of the US-Russian RUSALCA (Russian-American Long-term Census of the Arctic) program in 2004. Drawing on mooring, satellite, and hydrographic data, we summarize our current best understanding of the oceanography of the strait, starting with the underlying physics and reviewing the available, much newer and sparser, chemical measurements. Both the high productivity of the region and it being a constricted gateway to the Arctic make the strait a unique opportunity for observation of marine mammals transiting to the Arctic, and we discuss the first moored acoustic observations from marine mammal recorders in the strait. We conclude with a discussion of future challenges and plans for a long-term monitoring system for the Pacific Gateway to the Arctic.

CHALLENGES AND SOLUTIONS FOR WORKING YEAR-ROUND IN THE BERING STRAIT

The Unavoidable Challenges of Working in the Bering Strait

The challenges of measuring year-round in the Bering Strait are environmental, technical, and political.

The region is geographically remote, with the settlements in the area (e.g., villages of Diomedes and Wales; Figure 1c)

being accessible currently only by aircraft or by sea, although increasingly in recent years, plans for a tunnel or a bridge across the strait are frequently mooted, despite the lack of infrastructure on either side of the strait. Even access by sea is complex, as the nearest deepwater port is Dutch Harbor in the Aleutian Chain some 1,300 km south of the strait, while the closer port of Nome (220 km southeast of the Bering Strait) takes only smaller vessels and is vulnerable to closure in bad weather.

In winter (from approximately November/December to May/June), sea ice (and in places landfast ice) may block the strait (Torgerson and Stringer, 1985; Travers, 2012; author Woodgate and Cynthia Travers, University of Washington, unpublished data), hindering shipping but promoting sea-ice-based hunting and travel between the mainland and the islands. As discussed below, ice keels may be >20 m (Richard Moritz, University of Washington, unpublished data), endangering upper water column moored instrumentation. The catenary (i.e., here the underwater loop) of hawser (towing line) from tugs towing barges through the strait is another potential source of moored instrument loss. Due to the high productivity of the waters, biofouling of instrumentation (discussed further below) is also a major concern, and freezing water temperatures present further challenges to instrumentation.

The ~85 km wide strait is split into two channels by the two small Diomedes Islands (Little Diomedes: 4 km × 3 km, and Big Diomedes or Ratmanov Island: 8 km × 4.5 km) roughly in the center of the strait (title page graphic and Figure 1). While the channels are moderately flat and ~50 m deep, the sides of the channel and the islands are comparatively steep—about 15 m drop per kilometer on the sides of the strait, and about 50 m drop per kilometer by the islands (data from NOAA 2011 mapping survey, Kathleen Crane, NOAA, unpublished data). There is a shallow passage (probably less than 30 m deep) between

the islands. As discussed below, coastal currents are found on both the US and Russian coasts, and there are indications of trapped circulations around and near the islands (Woodgate and the RUSALCA 2011 Science Team, 2011; Raymond-Yakoubian et al., 2014; author Woodgate and colleagues, unpublished data).

The 1867 US-Russian convention line also runs through the Chukchi Sea and the center of the strait between the two islands at 168°58'37"W (Figure 1), meaning that Exclusive Economic Zone (EEZ) permission (US or Russian) is required to work in all regions of the strait.

Observations of the flow from explorers stretch back as far as 1728 (Coachman and Aagaard, 1966), where most, but not all, expeditions reported northward flow. Scientific measurements from the strait, although sparse in space and time, are reported as early as 1937 in the Russian literature (for discussion, see Shtokman, 1957). Although we appear to lack access to the full details of the Russian research from this era, it is clear that authors such as Ratmanov, Maksimov, and Leonov investigated in situ measurements, theory, and the broader role of the strait in the global ocean. By the middle of the twentieth century (Shtokman, 1957; Gudkovich, 1962; Coachman and Aagaard, 1966), a clearer picture was emerging of a strong (order 50 cm s⁻¹), generally northward current that was highly variable seasonally, strongly influenced by wind (especially on shorter time scales), and likely driven by some Pacific-Arctic sea-level difference (of unknown source), often termed the “pressure-head driven” flow. The roles of two coastal currents—the Siberian Coastal Current (SCC) on the Russian coast and the Alaskan Coastal Current (ACC) on the US coast—were also recognized. These insights into the structure and variability of the flow indicate the necessity for year-round measurements in the strait, preferably synoptic in both the US and Russian channels.

In September 1990, the joint US-USSR Circulation Study of the Chukchi Sea started an extensive mooring program

both in the strait and throughout the whole (US and Russian) Chukchi Sea, of which 13 moorings were successfully recovered in 1991 (Roach et al., 1995; Woodgate et al., 2005b). Within the strait proper, three mooring sites were established: A1 in the center of the Russian channel, A2 in the center of the US channel, and A3 in US waters mid-channel ~35 km north of the strait proper (Figure 1). Two more years of measurements both in US and Russian waters followed (1992–1993 and 1993–1994, albeit with mooring A3 placed some 200 km further north [site A3'] for three years starting in 1992), leading to the first direct measurements of the annual mean flow (0.8 ± 0.2 Sv) for the September 1990–September 1994 period and quantification of seasonal variability in transport and salinity (Roach et al., 1995).

However, 1994 marked a hiatus in moorings in Russian waters. Between 1994 and the advent of RUSALCA in 2004, although year-round measurements in the strait were continuous (with the exception of a one-year period, summer 1997–1998), they were only made in US waters.

In 2004, the US National Oceanic and Atmospheric Administration's (NOAA's) RUSALCA program was successful in obtaining the necessary permissions and clearances to deploy a year-round mooring in Russian waters at site A1, starting a new era in cross-strait measurements. In conjunction with US National Science Foundation (NSF)-funded International Polar Year and Arctic Observing Network (AON) projects supporting moorings in the US waters of the strait, from summer 2004 to summer 2011 a synoptic array of typically eight, but sometimes 11, moorings was deployed in the strait (with typically three moorings in Russian waters), giving high-resolution coverage of the velocity and water properties in both channels of the strait. Biofouling and battery issues dictate an annual servicing of the moorings. Moorings included both US and Russian instrumentation, providing data to allow for an intercalibration of

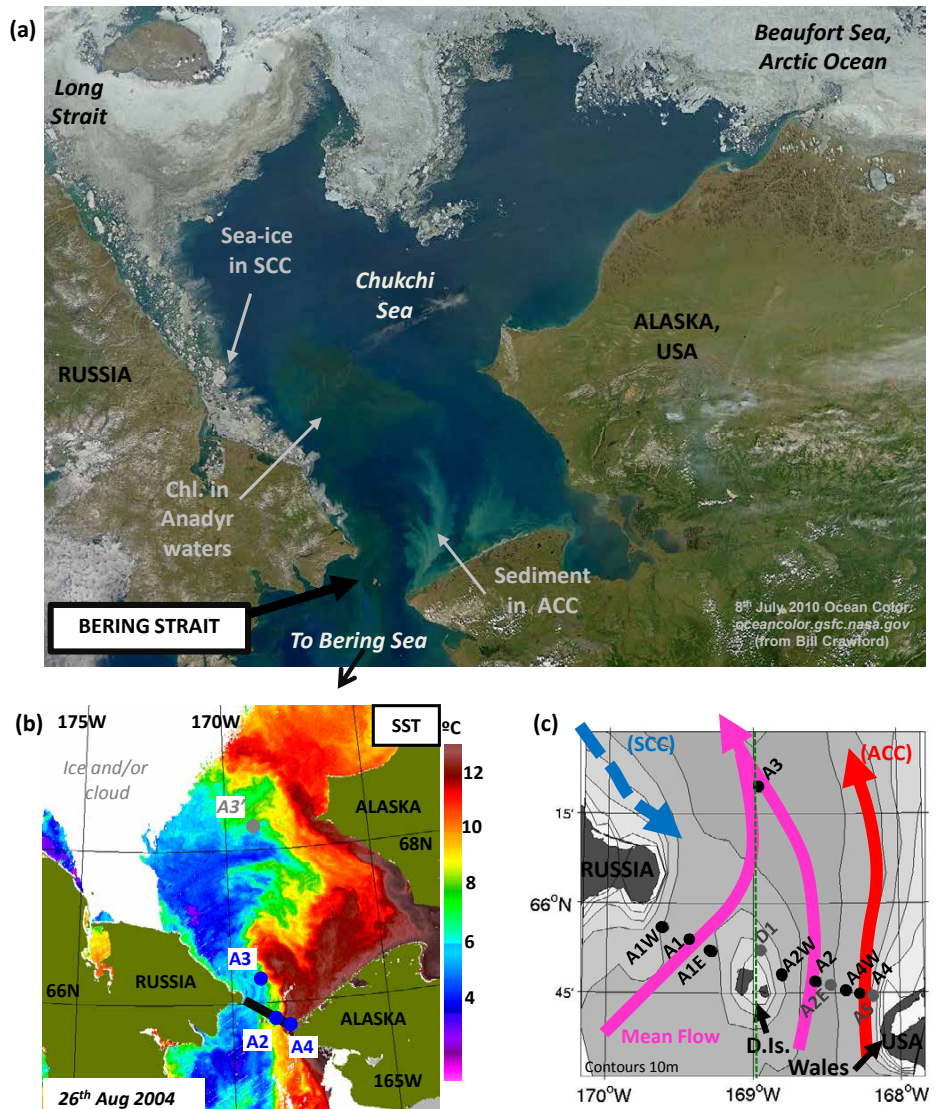


FIGURE 1. (a) July 8, 2010, ocean color (<http://oceancolor.gsfc.nasa.gov>) image of the Bering Strait and the Chukchi Sea (courtesy of B. Crawford). The Siberian Coastal Current (SCC) brings ice south into the Chukchi through Long Strait. North of the Bering Strait, ocean color suggests high chlorophyll (chl) in the Anadyr (Russian channel) Waters in the middle of the Chukchi Sea and sediment-rich waters in the Alaskan Coastal Current (ACC) in the southeastern Chukchi Sea. (b) August 26, 2004, Moderate Resolution Imaging Spectroradiometer (MODIS) sea surface temperature (SST) image (image courtesy of Mike Schmidt, from the Ocean Color Data Processing Archive, NASA/Goddard Space Flight Center, Greenbelt, MD) showing the extensive warm ACC waters in the eastern Bering Strait and Chukchi Sea, with mooring locations (Table 1) marked by dots (blue for the three moorings of the physical measuring system A2, A3, A4 and gray for the historic site A3') and by the black bar in the strait proper. (c) Schematic of the Bering Strait (with International Bathymetric Chart of the Arctic Ocean [IBCAO] bathymetry; Jakobsson et al., 2000) showing mooring locations (black/gray dots for multiple/single year deployments, respectively) and a schematic of annual mean flows: magenta = the mean flows through each channel, which combine at site A3; red = the ACC, found seasonally every year on the Alaskan coast; and blue = the SCC, found seasonally in some years on the Russian coast. D.Is. = Diomedes Islands (the village of Diomedede is located on Little Diomedede). Wales = village of Wales. The dashed vertical green line between the Diomedede Islands marks the US-Russian Exclusive Economic Zone (EEZ) border at 168°58'37"W.

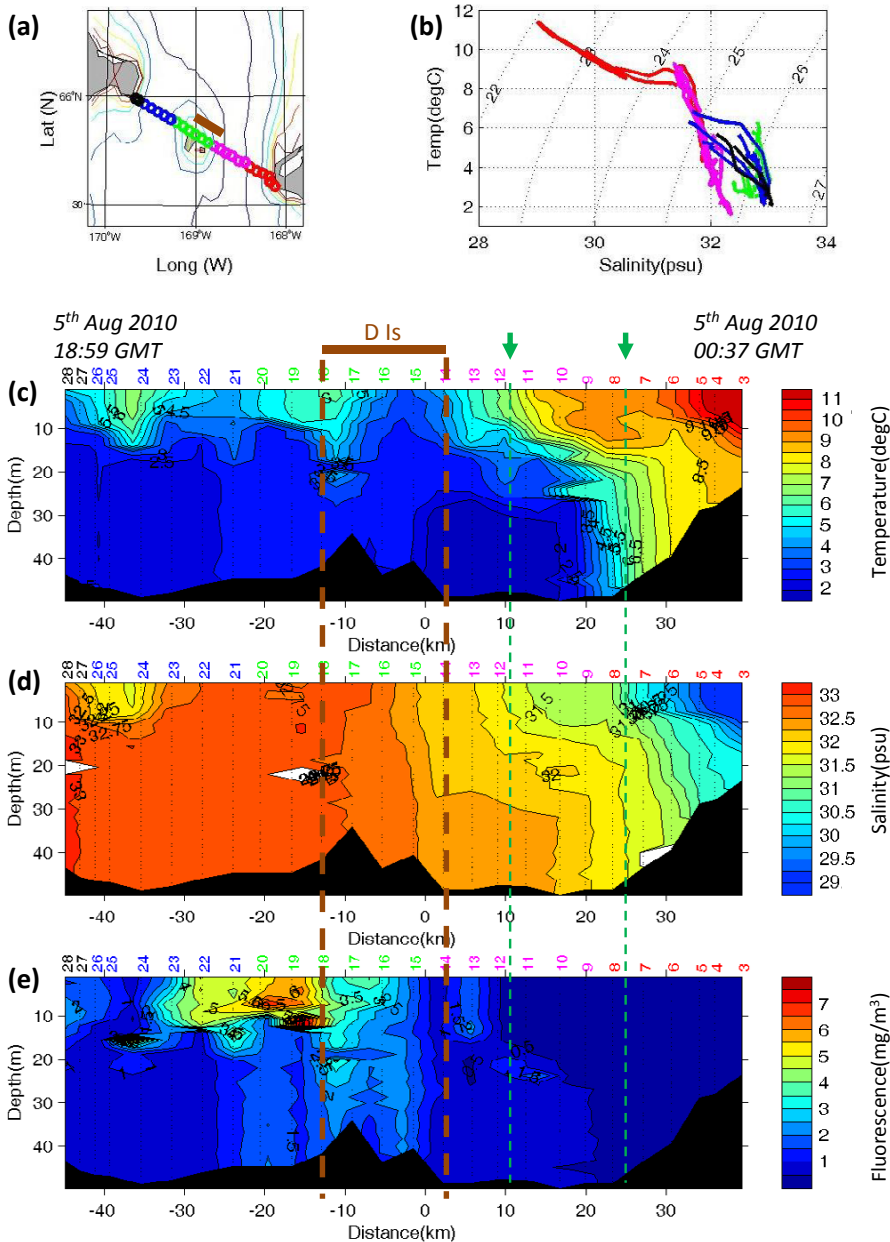


FIGURE 2. Bering Strait hydrographic section taken on August 5, 2010, from the vessel *Professor Khromov/Spirit of Enderby* (Woodgate et al., 2010a) under northward wind conditions, showing (a) map, (b) temperature-salinity distribution, and sections (looking north) of (c) temperature, (d) salinity, and (e) fluorescence. Colors on map, temperature-salinity (TS) diagram, and above the sections indicate station number. The brown bar above the sections indicates stations likely in the wake of the Diomed Islands (D Is), as discussed in the text. Dates give start and end times of the section. Distances are measured from the west side of the US channel (marked as E1 in Figure 5) to allow easy intercomparison with US channel figures (Figures 5 and 6c,d). Green arrows and vertical dashed lines mark locations of the currents identified by Native observations (Raymond-Yakoubian et al., 2014) discussed in the text. Warm, fresh, low fluorescence Alaskan Coastal Waters are found along the Alaskan coast (right). Note the approximately two-layer system in the rest of the strait, the increase of salinity toward the west (left), the subsurface fluorescence maxima in the Russian channel, and the anomalous waters behind (brown bar) the Diomed Islands.

data sets especially in the technology of current measurement. Joint US-Russian cruises brought together cross-border science teams (see <http://psc.apl.washington.edu/BeringStrait.html>), allowing for exchange of information otherwise inaccessible in the Russian literature, and free access to both EEZs allowed hydrographic sections to be taken across the entire strait (e.g., Figure 2).

Annual servicing of the high-resolution array in US waters continued until final recovery in 2013. However, clearance issues prevented the annual turnaround of the moorings in Russian waters in summer 2011, and although the Russian channel moorings were recovered in 2012, the two-year deployment and biofouling severely degraded data return. Due to continuing access issues, the Russian channel moorings were not redeployed until 2014, when one mooring was reinstated at the western edge of the Russian channel. Meanwhile, since prior work suggests that a particular set of three moorings in US waters is broadly sufficient to determine physical water properties and volume, heat, and freshwater fluxes through the strait (Woodgate et al., 2006, 2007; author Woodgate and colleagues, unpublished data), the US Office of Naval Research (ONR) and NSF-AON have funded these three moorings to be deployed in US waters starting in 2013 and to continue until summer 2018.

Table 1 summarizes all the US-related mooring deployments in the strait since 1990. The analysis of this extensive data collection is still ongoing, but we present preliminary results below.

The Advent of New and Interdisciplinary Mooring Technologies in the Bering Strait Region

A further advance of the recent years has been the introduction of newer technologies for measuring important parameters within the strait (Table 1).

For the first decade of the moorings (1990–2001), measurements were

taken with traditional Sea-Bird (SBE) SeaCAT (temperature and salinity) sensors and Aanderaa Recording Current Meters (RCMs) equipped with rotors. Despite typical preventative measures, both SeaCATs and RCMs were prone to biofouling, resulting in erroneously low salinities due to clogging of the salinity cells, or velocity dropouts due to slowing or jamming of the rotors (Roach et al., 1995; Woodgate et al., 2005b). As better technology became available, RCMs were replaced with their acoustic counterparts (2003–2005 onward), eliminating the rotor jamming issues. In 2002, an RDI acoustic Doppler current profiler (ADCP), also insensitive to biofouling, was introduced into the array in the new mooring A4, deployed first in 2001 to directly measure the ACC (Figure 1). The ADCP yields both a profile of velocity (as opposed to the point measurement of the RCM) and estimates of ice thickness and ice motion.

In 2007, the new ISCAT technology, developed at the Applied Physics Laboratory, University of Washington (APL, UW), was deployed for the first-ever year-round measurements of the upper water column. Before this time, all year-round measurements had been solely of the lower layer, since ice keels and shipping threatened instruments deployed within ~35 m of the surface. The strong currents of the strait precluded (and still preclude) the use of currently available winched sensors, and profilers climbing on a wire were also impractical, as the top float required would need to be in the ice-risk zone. In the ISCAT system, a Sea-Bird temperature-salinity-pressure sensor is contained in a top “ice-resistant” float, which is placed in the upper water column. The data from this instrument are telemetered every 30 minutes via an inductive modem to a data logger placed at a safe depth on the mooring. The buoyancy of the top ice-resistant float is designed so that the float will pull down under ice keels. If, nonetheless, the top float (which is connected to the rest of the mooring via a weak link) is severed

from the mooring by the ice, the logger will retain the data recorded up to the time of instrument loss. These ISCAT instruments, deployed successfully on typically three to five moorings per year from 2007 to present day, combined with satellite sea surface temperature measurements, allow us to assess year-round temperature and salinity structure in the water column (as discussed below).

The importance of the high level of nutrients in the strait has driven attempts at in situ moored measurements of nitrate, first with the EnviroTech NAS Nutrient Analyzer sensors (2000–2003) and then more recently (and successfully) with the Satlantic ISUS (In Situ Ultraviolet Spectrophotometer) instruments (2005 to 2014). In 1999, mooring A3 also carried a prototype 12-bottle moored water sampler (MITESS, Moored Trace Element Serial Sampler; Bell et al., 2002), set to take a water

sample once every month (Kelly Falkner, OSU, unpublished data; Woodgate, 2000). Bio-optic sensors (fluorescence, turbidity, and, sometimes, PAR [photosynthetically active radiation]) have been mounted on pumped Sea-Bird sensors or as independent stand-alone instruments since 2002 and, for two years starting in 2011, prototype ocean acidification sensors (measuring pH and $p\text{CO}_2$) were also deployed at site A3. Also, in consideration of higher trophic levels, marine mammal acoustic recorders have been deployed on the moorings since 2009. Below we discuss preliminary results from all these sensors.

Biofouling—One Oceanographer’s Signal is Another Oceanographer’s Noise

Before reviewing the mooring knowledge gained by these decades of moorings, we reflect briefly on unintended

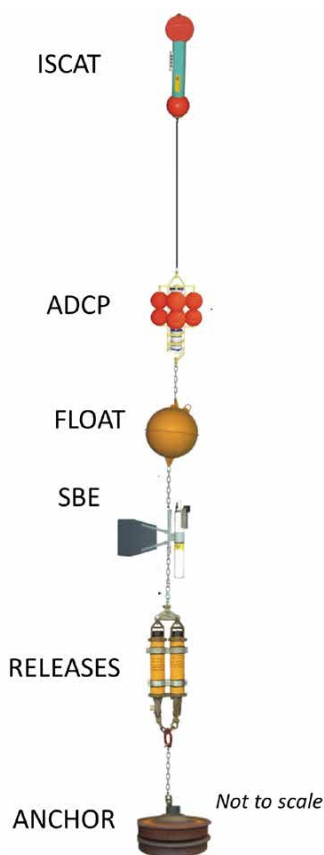


FIGURE 3. Typical Bering Strait mooring design from 2007 onward (not to scale). Image courtesy of Jim Johnson, University of Washington



FIGURE 4. Recovery of mooring A3-03 (deployed from July 2, 2003, to August 31, 2004), showing heavily biofouled trifloat-flotation package (upper item) and NAS instrument package (bottom of photo). Photo credit: Rebecca Woodgate, University of Washington, taken from R/V Alpha Helix

TABLE 1. Bering Strait mooring positions and instrumentation from 1990–2014. Column gives mooring location. Row gives year and month of deployment. Italic entry means data quality not known. “Bottom depth” gives average (av), minimum (min), and maximum (max) of water depth at each mooring site, with average being the average over available years. Instruments collecting no useful data are not included. TS = lower layer (~45 m) temperature (T) and salinity (S). V = lower layer (~45 m) Aanderaa single point current meter. AV = lower layer (~45 m) Acoustic Aanderaa single point current meter. Turb = lower layer (~45 m) Acoustic Aanderaa single point current meter with turbidity. AARI = lower layer (~33 m) Russian single point current meter. Vect = lower layer (~38 m) Russian vector single point current meter. BP = bottom pressure sensor. ULS = Upward Looking Sonar. MITES = Water sampler. NAS = Nutrient Analyzer. ISUS = Nitrate meter. Opt = Biooptics (e.g., some of fluorescence, turbidity, transmissivity, and photosynthetically active radiation [PAR]). FLT = fluorescence and turbidity. WR = marine mammal acoustic recorder. pH = SAMI and SeapHox pH meters. ISCAT = upper layer (~15–18 m) temperature and salinity sensor.

MOORING	A1W (A12)	A1 (A11)	A1E (A13)	D1	A2W	A2	A2E	A4W	A4	A5	A3	A3'
NOMINAL POSITION	65°56.0'N 169°37.0'W	65°54.0'N 169°26.0'W	65°52.0'N 169°17.0'W	65°52.2'N 168°56.8'W	65°48.0'N 168°48.1'W	65°46.9'N 168°34.1'W	65°46.3'N 168°28.1'W	65°45.4'N 168°22.0'W	65°44.8'N 168°15.8'W	65°44.4'N 168°11.1'W	66°19.6'N 168°57.5'W	68°10'N 168°58'W
BOTTOM DEPTH av (min, max)	51 m (48–54 m)	51 m (48–52 m)	50 m (48–51 m)	47 m	53 m (51–55 m)	55 m (52–57 m)	57 m	55 m (54–56 m)	48 m (47–50 m)	45 m	57 m (54–59 m)	57 m (56–59 m)
1990 (Sept)		A1-90 TS V BP				A2-90¹ TS V BP					A3-90 TS V BP	
1991 (Sept)						A2-91 TS V BP					A3-91 TS V BP	
1992 (Sept)		A1-92 ULS TS V BP				A2-92 ULS T V BP						A3'-92 ULS T V BP
1993 (Sept)		A1-93 ULS TS V				A2-93 - TS V						A3'-93 ULS TS V
1994 (Sept)						A2-94 ULS TS V						A3'-94² ULS TS V
1995 (Sept)						A2-95 ULS TS V						
1996 none												
1997 (July)						A2-97 ULS TS V					A3-97 ULS TS V	
1998 (July)						A2-98 TS					A3-98 TS V	
1999 (July)						A2-99 ULS TS V -					A3-99 ULS TS V MITESS	
2000 (Aug/Sept)						A2-00 ULS TS V -					A3-00 ULS TS V NAS	
2001 (Sept)						A2-01 ULS TS - -			A4-01 - TS V -		A3-01 ULS TS AV NAS	
2002 (Jun)						A2-02 ULS TS V -			A4-02 - TS ADCP -		A3-02 ULS TS AV NAS Opt	
2003 (July)						A2-03 ULS TS V -			A4-03 - TS ADCP -		A3-03 ULS TS AV NAS Opt	
2004 (Aug/Sept)		A1-04³ TS AV Opt				A2-04 ULS TS V -			A4-04 - TS ADCP -		A3-04 ULS TS AV Opt	
2005 (July & Aug)	A1W-05 - TS AV ISUS Opt	A1-05 - TS ADCP -	A1E-05 - TS AARI			A2-05 ULS TS V ISUS Opt			A4-05 - TS ADCP -		A3-05 ULS TS AV -	

Table continues next page...

consequences. Although biofouling (see, e.g., Figure 4) was/is primarily a nuisance for the physical measurements (requiring at times dragging for moorings since a small, unfortunately located barnacle can successfully jam the mooring release mechanism—see photos in cruise reports available at <http://psc.apl.washington.edu/BeringStrait.html>), over the decades of work, it became clear

even to the physical oceanographic center, that the nature of the biofouling on the recovered moorings was changing (Woodgate and the RUSALCA 2012 Science Team, 2012). Thin bryozoans gave way to extensive barnacles; mussels were found at depth in instrument cages; basket stars occasionally were recovered with the instruments; and in 2012 even amphipods were found on the moorings

(Marnie Zirbel, Oregon State University, *pers. comm.*, 2012). Inadvertently thus, the moorings offer a platform for assessing species shifts over the last decades. Photographic documentation of these shifts is available in the cruise reports (and by application to the lead author) to any interested parties.

TABLE 1. Continued...

MOORING	A1W (A12)	A1 (A11)	A1E (A13)	D1	A2W	A2	A2E	A4W	A4	A5	A3	A3'
NOMINAL POSITION	65°56.0'N 169°37.0'W	65°54.0'N 169°26.0'W	65°52.0'N 169°17.0'W	65°52.2'N 168°56.8'W	65°48.0'N 168°48.1'W	65°46.9'N 168°34.1'W	65°46.3'N 168°28.1'W	65°45.4'N 168°22.0'W	65°44.8'N 168°15.8'W	65°44.4'N 168°11.1'W	66°19.6'N 168°57.5'W	68°10'N 168°58'W
BOTTOM DEPTH av (min, max)	51 m (48–54 m)	51 m (48–52 m)	50 m (48–51 m)	47 m	53 m (51–55 m)	55 m (52–57 m)	57 m	55 m (54–56 m)	48 m (47–50 m)	45 m	57 m (54–59 m)	57 m (56–59 m)
2006 (July & Aug)	A1W-06 - TS AV AARI ISUS Opt	A1-06 - TS ADCP -	A1E-06 - TS V AARI -			A2-06 ULS TS AV - ISUS Opt			A4-06 - T ADCP -		A3-06 ULS TS AV -	
2007 (Aug)	A1W-07 - TS AV ISUS Opt	A1-07 ISCAT TS -	A1E-07 - TS AV AARI		A2W-07 ISCAT TS ADCP BP	A2-07 ISCAT TS ADCP ISUS Opt		A4W-07 ISCAT TS ADCP -	A4-07 ISCAT TS ADCP BP		A3-07 ISCAT TS ADCP -	
2008 (Oct)	A1W-08 - TS AV ISUS Opt	A1-08 ISCAT TS ADCP -	A1E-08 - TS AV AARI		A2W-08 ISCAT TS ADCP BP	A2-08 ⁴ ISCAT TS ADCP ISUS Opt			A4/R-08 ⁵ ISCAT TS ADCP BP		A3-08 ISCAT TS ADCP -	
2009 (Aug)	A1W-09 - TS AV ISUS Opt	A1-09 ISCAT TS ADCP -	A1E-09 - TS AVTurb AARI		A2W-09 ISCAT TS ADCP WR BP	A2-09 ISCAT TS ADCP ISUS Opt		A4W-09 ISCAT TS ADCP -	A4-09 ISCAT TS ADCP BP		A3-09 ISCAT TS ADCP WR	
2010 (Aug)	A1W-10 - TS AV ISUS Opt BP	A1-10 ISCAT TS ADCP -	A1E-10 - TS AV AARI		A2W-10 ISCAT TS ADCP FLT WR -	A2-10 ISCAT TS ADCP ISUS Opt -		A4W-10 ISCAT TS ADCP -	A4-10 ISCAT TS ADCP BP FLT -		A3-10 ISCAT TS ADCP -	
2011 (Jul)	A1W-10 continued ISUS Opt	A1-10 continued TS ADCP	A1E10 continued TS AARI	D1-11 - TS AV Vect WR	A2W-11 ISCAT TS ADCP FLT WR BP	A2-11 ISCAT TS ADCP ISUS Opt -	A2E-11 ISCAT TS ADCP -	A4W-11 ISCAT TS -	A4-11 ISCAT TS ADCP FLT BP	A5-11 - TS AVTurb -	A3-11 ISCAT TS ADCP ISUS Opt WR pH	
2012 (July)					A2W-12 ISCAT TS ADCP WR BP -	A2-12 ISCAT TS ADCP ISUS Opt -		A4W-12 ISCAT TS ADCP WR -	A4-12 ISCAT T ADCP BP -		A3-12 ISCAT TS ADCP ISUS Opt FLT WR BP	
2013 (July)						A2-13 ISCAT TS ADCP ISUS Opt WR			A4-13 ISCAT TS ADCP - WR		A3-13 ISCAT TS ADCP ISUS Opt WR	
2014 (July)	A1W-14 In water					A2-14 In water			A4-14 In water		A3-14 In water	

Notes:

¹Additional ADCP mooring deployed in 1990 ~8 km north of A2-90.

²Additional ULS mooring deployed in 1994 ~9 km south of A3-94.

³Additional Russian mooring deployed ~13 km east of A1-04.

⁴A2-08 deployed ~750 m from usual position.

⁵ Mooring A4-08 broke on deployment, second mooring A4R-08 deployed at same site.

THE PHYSICAL OCEANOGRAPHY OF THE BERING STRAIT FROM 24 YEARS OF MOORINGS (1990–2014)

The Summer Bering Strait: Flow and Hydrography

On a pleasant summer day in the Bering Strait, one might expect light ($0\text{--}10\text{ m s}^{-1}$) northward or southward winds (data from National Centers for Environmental Prediction, <http://www.ncep.noaa.gov>), low sea state, and anything from fog to cross-channel visibility. The results of Figure 2, showing various parameters from a hydrographic section across the strait taken on such a day in 2010 (August 5, 2010), are typical of many of the summer features of the Bering Strait hydrography. On average, as long as winds are northward, or less than

$\sim 10\text{ m s}^{-1}$ southward (Woodgate et al., 2005b), the flow through the strait is northward, and typically $\sim 30\text{ cm s}^{-1}$ (on this day, actually $\sim 40\text{ cm s}^{-1}$). On similar days (e.g., Figure 5), ship's ADCP and moored ADCP data show a strongly uniform, mostly barotropic (invariant with depth) current throughout the strait, with flow intensification on the US side near the surface near the coast (author Woodgate and colleagues, unpublished data). Due to the narrowness of the strait, the flow is strongly rectilinear (i.e., along-channel, approximately northward or southward; Woodgate et al., 2005b), although with exceptions we discuss below.

In terms of water properties, the most dominant feature of the system is warm, fresh waters on the Alaskan coast, waters originating from the ACC (Coachman et al., 1975; Woodgate and Aagaard, 2005). Waters in the west (i.e., the Russian channel) are typically colder than the ACC, although may be warmer than mid-strait waters, and there is a ubiquitous, strong east-west

salinity gradient, with saltier waters on the Russian side (Coachman et al., 1975).

By drawing on hydrographic CTD (conductivity-temperature-depth) sections taken across the strait every summer/fall from 2000 to 2014 and mooring data, we can identify other persistent features of the water properties in the strait.

Under northward wind conditions, the westward extent of the warm Alaskan Coastal Waters (ACW), viz., waters that are or were once part of the dynamically coastally trapped ACC, is remarkably consistent between sections, with extents being typically $10\text{--}20\text{ km}$ out into the strait. This length scale is, unsurprisingly, close to a typical Arctic Rossby radius (order 10 km). There is, again unsurprisingly, a geostrophic velocity maximum associated with the edge of these waters, resulting in a change of velocity with depth of order 50 cm s^{-1} , to which must be added the bottom flow of order $20\text{--}40\text{ cm s}^{-1}$ to obtain the total velocity in the strait (Figure 5). The fresher, warmer waters extend to depths of 40 m by the coast, thinning toward the westward

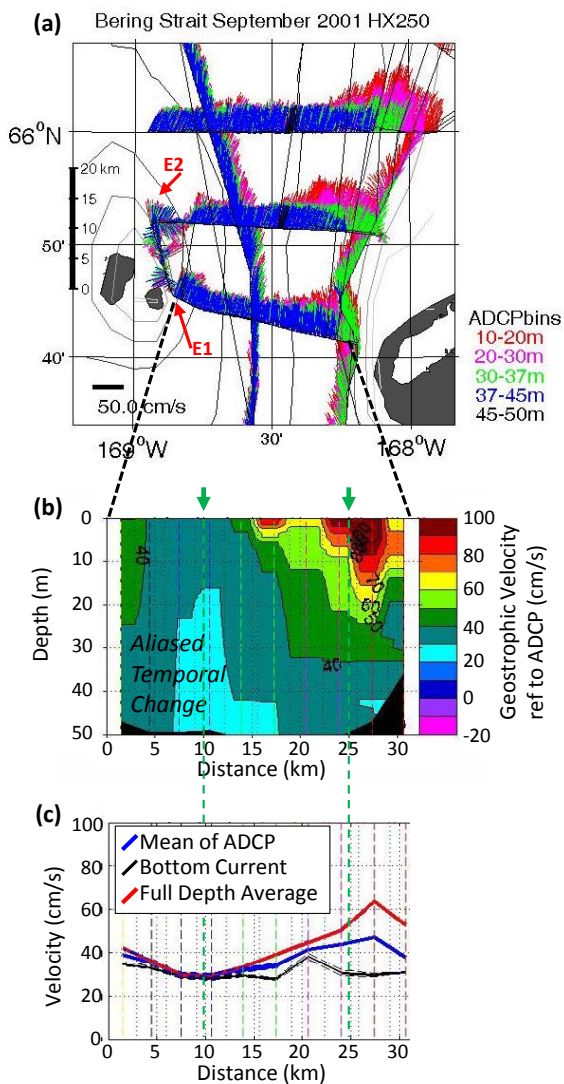


FIGURE 5. Velocities in the Bering Strait on September 11–12, 2001, from R/V *Alpha Helix* (Woodgate, 2001), taken under generally northward wind conditions, with winds turning weakly southward midway through survey. (a) Map with colored sticks indicating water velocity measured by the ship's acoustic Doppler current profiler (ADCP) on sections in and north of the strait. Colors indicate depth of ADCP velocity bins (shallowest bin $\sim 15\text{ m}$ in red, deepest bin $\sim 40\text{--}50\text{ m}$ in blue or black as per legend), length and direction represent speed and direction. Velocity always decreases with depth, and thus, since sticks are plotted from the surface downward (i.e., with deeper bins overprinting shallower bins), blue/black regions indicate areas of barotropic (invariant with depth) flow. E1 and E2 mark the permanent eddy zones discussed in the text. (b) Section (looking north) of geostrophic velocity in the US channel (calculated from concurrent CTD section) referenced to the ship's ADCP data, allowing extension of the ADCP velocity profiles up to the surface. (c) Variation across the strait of the mean of the ADCP velocity (blue), the bottom flow inferred from the referenced geostrophic velocity (black, with dashed lines indicating uncertainty in fit), and full-depth averaged flow (red). In (b) and (c), distance is eastward from the start of the CTD section in the west of the US channel, approximately at the point marked E1 in (a). Vertical lines at $\sim 3\text{ km}$ spacing indicate station locations. Green arrows and vertical dashed lines mark the currents identified by Native observations (Raymond-Yakoubian et al., 2014), as discussed in the text. In all these panels, the Alaskan Coastal Current appears as intensified flow near the surface on the US coast (right). Note that mooring data from the ~ 3 hours during which the section was taken show that, over this period, lower-layer velocities mid-strait fell from $\sim 30\text{ cm s}^{-1}$ (at the time of the westernmost part of the section) to $\sim 20\text{ cm s}^{-1}$ (by the eastern end of the section), and this temporal change is aliased into apparent spatial variability, as indicated in (b). (No ship's ADCP data are available from the Russian channel.)

edge of the current in the wedge structure, typical of coastally trapped buoyant currents (Figure 2).

Under stronger southward wind conditions (or just following such southward wind events), section and moored ADCP data (Figure 6 and author Woodgate and colleagues, unpublished data) indicate that ACW move (or have moved) away from the coast and across the strait.

This cross-strait circulation is consistent with Ekman dynamics, with surface waters being driven to the right of the wind direction, and, in fact, in the full-depth moored ADCP records, it is sometimes possible to see a clear component of westward flow in the near-surface layers and compensating eastward flow at depth (illustrated schematically by red arrows in panel d in Figure 6). The result of this

is to “spill” warm fresh waters across the strait, at times reaching at least as far as the Diomedede Islands (e.g., September 2007; Woodgate, 2008).

This mechanism is at least in part responsible for another key feature of the strait, viz., the approximately two-layer structure of the water column, i.e., an upper warmer (and frequently, but not always, fresher) 10–20 m thick layer

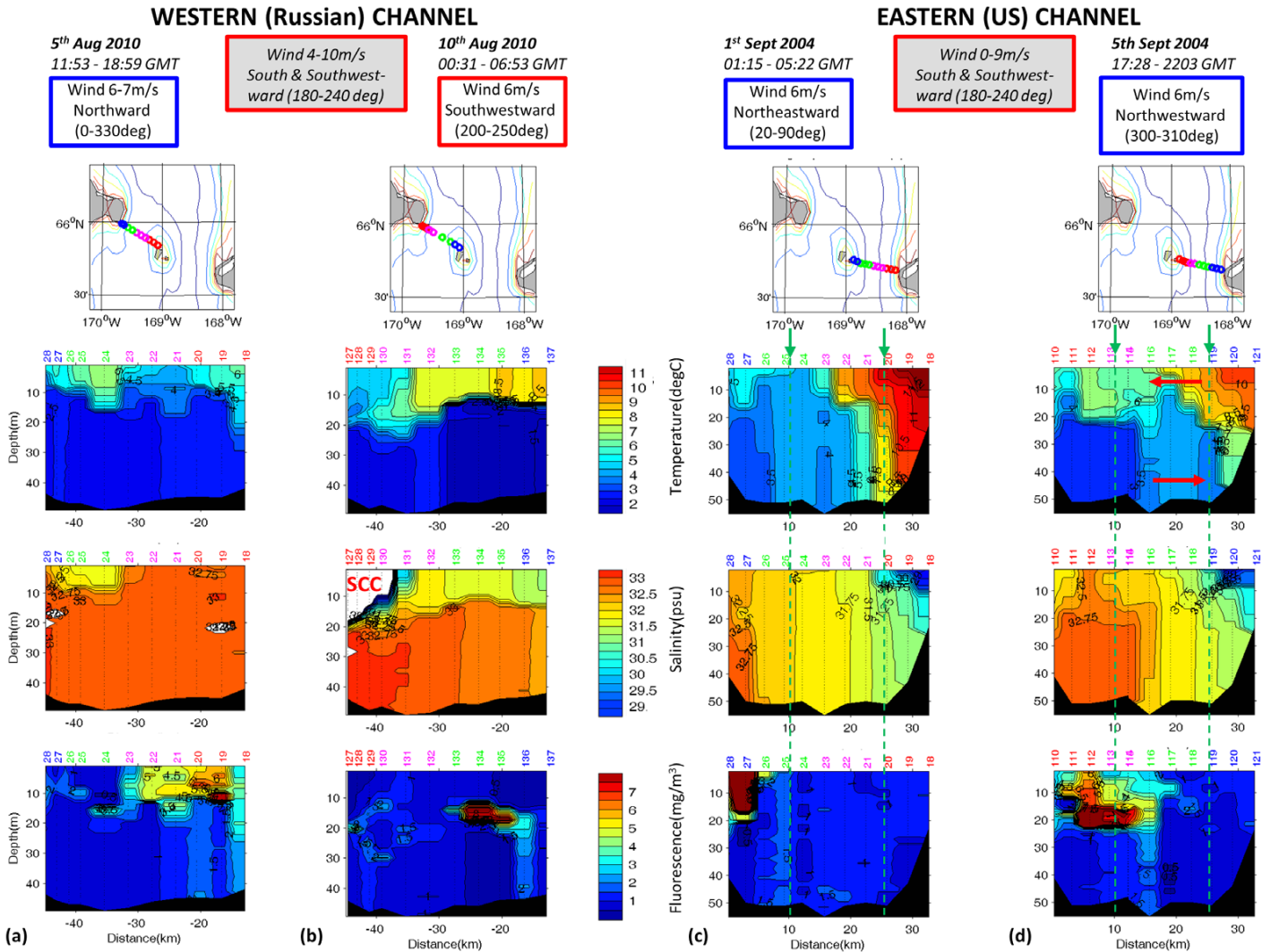


FIGURE 6. Repeats of Bering Strait hydrographic sections (looking north) taken ~5 days apart in the Russian channel (August 2010, columns a and b) and the US channel (September 2004, columns c and d), with map and sections as per Figure 2. Text in boxes above maps give National Centers for Environmental Prediction (NCEP) wind conditions (color-coded such that the blue-framed box indicates northward wind, and the red-framed box indicates southward wind) for the time of the section (above each section) and between the sections (gray box in italics between sections), showing in each case the wind turning southwards after the first section. Data in panel (b) are taken under southward wind conditions. Data in panel (d), although from northwesterly wind conditions, are taken just following a southward wind event. Distances are from the west side of the US channel, as in Figures 2 and 5. Green arrows and vertical dashed lines mark the currents in the US channel identified by Native observations (Raymond-Yakoubian et al., 2014). Both channels show, over this short time period, significant changes in structure and values for temperature, salinity, and fluorescence. In the Russian channel, the second occupation (column b) under strong southward wind conditions, shows the Siberian Coastal Current (SCC) reaches the strait with salinities of 24 psu (red label in middle section). In the US channel, the second occupation (column d), taken just after southward wind conditions, shows the waters of the Alaskan Coastal Current to have spilled westward across the strait, as discussed in the text. The magnitude of these short-time-period changes illustrates the challenges of interpreting single section data.

above a more homogeneous colder saltier layer reaching to the bottom, present through much of the strait (Figures 2 and 6). As we will see below, this layered structure is also manifest in the biological properties. While the “spilling” of ACW is a good candidate mechanism for creating this two-layer structure, it is also notable that in some cases (e.g., data from 2001, 2003, and 2006, not shown), the upper layer is marked mostly in temperature and hardly in salinity, suggesting solar heating of the upper water column contributes significantly.

Over the years, biological parameters—fluorescence, dissolved oxygen, and transmissivity (some shown in Figures 2 and 6)—have been measured on some sections. Very typical of the region are subsurface maxima in fluorescence, which often match the base of the two-layer structure described above. Fluorescence values are also standardly low in the ACC and increase westward in the more nutrient-rich waters of the Russian channel, although the distribution is often patchy. High values are also often found near the islands. High dissolved oxygen values are

also found in the middle/west of the US channel (we lack oxygen data from the Russian channel), with waters frequently appearing significantly (several tens of percent) supersaturated (Woodgate and the RUSALCA 2012 Science Team, 2012; Woodgate et al., 2014), although without bottle calibrations of the CTD sensors, quantitative numbers should be interpreted with caution.

It is gratifying to compare these snapshots with the much longer-term, indigenously assessment of the velocity in the strait, documented in Raymond-Yakoubian et al. (2014), who interviewed Native peoples from the US and Russian coasts of the Bering Strait and Chukchi Sea. Their summarizing map shows three distinguishable currents in the US channel at ~30 km, ~15 km, and ~7 km off Wales, Alaska (equivalent to ~10 km, 25 km, and 33 km on Figures 2, 5, and 6). Our sections are generally not close enough to shore to identify the current nearest Wales, however the middle current matches well the location in our sections of the edge of the ACW and the associated surface intensified velocity

(identified from ship’s ADCP data or geostrophic velocity, e.g., Figure 5), typically found between ~25–30 km on our sections (equivalent to ~10–15 km off Wales). We hypothesize that the current furthest from Wales is a manifestation of the main flow through the channel. The Native communities also note that waves (and thus also winds) from the north or northwest bring crabs and clams ashore in Wales, consistent with the compensating eastward flow at depth driving upwelling along the coast during the “spilling” events discussed above.

Ubiquitous to all this work are the rapid and large variations that can occur in the region at times of changing wind (Figure 6). Mooring data allow us to quantify variations in flow and temperature-salinity (TS) properties over the time taken to run sections, and indicate that a section must be run over a few hours (not a day) to be considered synoptic. For example, although early published velocity sections from the entire strait (Coachman et al., 1975) show strong cross-strait variability, it is almost certain (as indeed suggested by the authors), that this variability is just the result of aliasing temporal change, and that within the strait proper (i.e., away from the islands or the coasts), the flow field is mostly homogeneous (Figure 5). This often-overlooked fact is vital to meaningful interpretation of hydrographic data from the region.

The Seasonal Boundary Currents: The Alaskan Coastal Current (ACC) and the Siberian Coastal Current (SCC)

As is clear from Figure 1, the spatial variability of water properties in the Chukchi Sea in summer is dominated by the presence of two coastal currents, the Alaskan Coastal Current and the Siberian Coastal Current.

As described above, the ACC and the waters (ACW) from the ACC are signature features also in the Bering Strait proper. The warm, fresh ACC (Figures 2, 5, 6, and 7) is likely the consequence of significant riverine influence, and is high

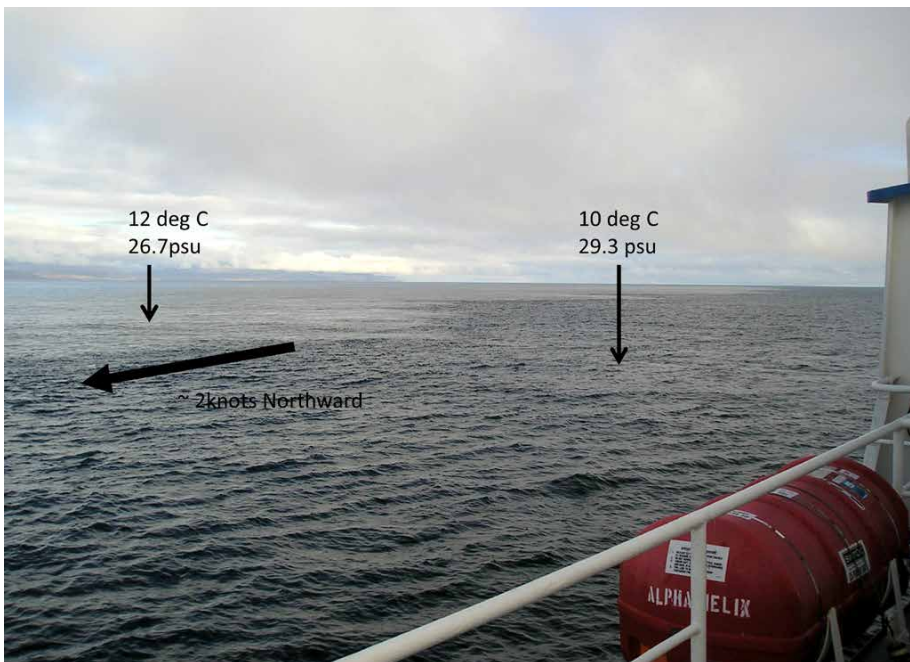


FIGURE 7. The Alaskan Coastal Current (smoother waters away from the ship) off Cape Prince of Wales, Alaska, on September 5, 2004, at 65°30.29'N, 168°4.08'W (~6 km offshore), annotated with R/V *Alpha Helix* underway surface data (~4 m depth for temperature and salinity, ~10 m depth for velocity). Photo credit: Rebecca Woodgate, University of Washington

in sediment and low in nutrients. It is present seasonally from approximately late April to late December and can be tracked northward through the Chukchi Sea and eastward along the northern coast of Alaska (Paquette and Bourke, 1974; Ahlnäs and Garrison, 1984; Woodgate and Aagaard, 2005). Indeed, ACW are also found (possibly after a transit time of ~2 years) in the Canadian Basin of the Arctic (Jackson et al., 2011). Although the volume transport of the ACC (~0.1Sv) is small compared to the full Bering Strait throughflow (~0.8 Sv), since it is significantly warmer (>5°C) and fresher (>7 psu) (Figures 2 and 6) than the main waters of the strait, it is estimated to carry about one-third of the heat and one-quarter of the freshwater flux of the strait (Woodgate et al., 2006). Undoubtedly, the ACC also varies interannually, although this aspect has been only rarely (or indirectly) addressed (Woodgate et al., 2006; Brugler et al., 2014).

On the Russian coast, the SCC is much less observed by in situ measurements (e.g., Figures 6 and 8, and Weingartner et al., 1999). The cold, fresh SCC, also seasonal and of volume transport ~0.1 Sv, originates in the East Siberian Sea, and in some (but not all) years flows southward into the Chukchi Sea via Long Strait (Münchow et al., 1999; Weingartner et al., 1999). Often carrying sea ice (e.g., Figure 1), the SCC extends southward along the Russian coast until usually being deflected into the central Chukchi Sea by winds and/or northward-flowing Bering Strait waters. Only rarely (under conditions of strong southward wind) does the SCC reach the Bering Strait (Weingartner et al., 1999; Woodgate et al., 2010a; see Figure 6).

Eddy Zones and Trapped Circulations Around the Islands

It is important to note that the sections shown in Figures 2, 5, and 6 all run slightly to the north of the Diomede Islands, and anomalous waters and flow properties are usually encountered in this region, which is effectively in the wake of the islands

during times of northward flow (author Woodgate and colleagues, unpublished data). While (as discussed above) ADCP sections show fairly uniform northward flow throughout the channels of the strait (data shown are only from the US channel, but mooring data indicate strong flow coherence across the Russian channel also), in contrast an eddying region is found north of the islands in the last stations in US waters (Figure 5, marked E1 and E2). This conclusion is strongly supported by satellite sea surface temperature (SST) data (e.g., title page graphic), which show cold, trapped eddies behind the islands. Mooring D1-11 was deployed in 2011 to quantify the year-round presence of these features and their role in mixing within the strait (author Woodgate and colleagues, unpublished data).

Mixing caused by eddies shed by flow past an island is known, in suitable circumstances, to cause phytoplankton blooms (e.g., Hasegawa et al., 2009), and in our summer surveys, at least qualitatively, there were larger concentrations of birds in this region compared to in either channel of the strait at comparable distances from the islands. Moreover, Native traditions (Raymond-Yakoubian et al.,

2014) warn of dangerous eddying zones ~8 km and ~25 km northeast/north of the islands. The closer of these could be a feature in the eddy zones E1 and E2 (Figure 5), while the more distant eddy (approximately three times the length of Big Diomede away from the islands) could relate to features seen in SST maps (e.g., title page graphic).

Thus, it can be assumed that due to some form of island trapping, waters close to and behind the islands may have somewhat different properties than waters in the main channels of the strait, as is evident to some degree in Figure 2.

The Winter Bering Strait: Flow, Hydrography, and Its Relationship to the Seasonal Cycle

Using a combination of ~45 m deep mooring data, ISCAT data from ~15 m deep, and SST satellite data, we can track the transition of the water column into winter. Shortwave solar radiation input starts to decline in July, falling to near zero by the end of October. Water temperatures lag this change, starting to cool only in September/October (Woodgate et al., 2010b). Although in summer, warmer fresher waters are at the surface, surface



FIGURE 8. The Siberian Coastal Current (light blue waters near the coast) on August 25, 2012, just off Cape Dezhnev (showing also monument to Semyon Dezhnev on land). *Photo credit: Aleksey Ostrovskiy, RUSALCA*

cooling in autumn leads to a temperature inversion in the strait, with colder waters overlying saltier warmer waters. The water column then homogenizes. We assume this homogenization is primarily due to wind-driven or related flow-driven mixing, since from the salinity stratifications found in summer (Figure 2) it is clear that cooling alone is insufficient to mix the entire water column. Note that the cooling trend is associated with freshening of the deeper layers, as the surface fresher layers are mixed down to the depths of the lower layer instruments (Woodgate et al., 2005a).

Typically, by late December, the water column cools to freezing, sea ice appears, and subsequent ice growth through the winter drives salinization of the waters by brine-rejection until about March, when spring melt and/or advection of waters from the south start to freshen the water column at the freezing temperature (Woodgate et al., 2005a). As sea ice disappears in May/June, the water column starts to warm. SST data indicate the surface warms faster than at depth, but ISCAT data suggest that for approximately one month, the warmer surface layer is shallower than 15–20 m, since only after that time do ISCAT temperatures diverge from lower layer temperatures. For quantification of the seasonal cycles in lower layer temperature and salinity, see Woodgate et al. (2005a).

Although this description is primarily one-dimensional (i.e., here assuming everything is locally driven from the surface and there is no horizontal variability), the effects of advection on the water properties of the strait must not be neglected. Indeed, it is hypothesized that oceanic advection of heat from the south both hinders ice formation in the fall and affects ice melt in the summer (Woodgate et al., 2012). While the focus of our paper is in describing the oceanography of the strait itself, the water properties are certainly strongly influenced in some complex manner by the Bering Sea to the south, not just by local effects, and the flow field is, as discussed above,

frequently related to pressure gradients from the Pacific to the Arctic or to global wind effects.

In addition to these strong seasonal changes in temperature and salinity (which in turn affect density and thus equilibrium depth for these waters in the Arctic water column), there is also a seasonal change in velocity, with winter currents generally being weaker northward or sometimes even southward (Woodgate et al., 2005a). This reflects that the winter winds are more southward and oppose the northward pressure-head-driven flow (Woodgate et al., 2005b), an understanding also clearly recognized in the Native knowledge of the region (Raymond-Yakoubian et al., 2014).

During winter, (in contrast to the large summer cross-channel variability in temperature and salinity) mooring data suggest that all of the Bering Strait region (and most of the Chukchi Sea) is at the freezing temperature with only a small variation in salinity (Figures 11 and 12 of Woodgate et al., 2005b). Indeed, from the entire mooring data set (not shown), salinity differences in winter between the Russian and the US channels are, on average, less than 0.5 psu, although there is some indication of greater cross-strait variability in recent years. Although the velocity shear and variability in temperature across the eastern channel associated with the ACC generally disappears with the arrival of freezing waters, at ~40 m depth at site A4 we do find episodic freshenings of order 1 psu even in the middle of winter, and winter ISCAT data (~15 m deep) similarly show short events of near-surface freshening.

Sea Ice in the Bering Strait

In situ measurements of sea ice have been another long-term goal. As early as 1992, prototype Applied Physics Laboratory (APL) upward-looking sonars (ULS) were deployed in the strait to determine the sea-ice thickness distribution (Richard Moritz, University of Washington, unpublished data). In a more recent innovation (Travers, 2012),

ADCP data from the strait have been used to assess both ice thickness and ice flux. While the ADCP data are less accurate than ULS data, Travers (2012) estimates that of the ~0.5 m error in the individual measures of ice thickness from the ADCP, ~50% is due to the beam footprint error (viz., that the sonar illuminates an area of ice of nonuniform thickness), which remains an issue even with dedicated ice sonars (Vinje et al., 1998). ADCP results from winter 2007–2008 identify ice keels of up to 16 m depth and mean ice thickness over the winter of ~1.5 m (Travers, 2012). Brine rejection from this thickness of ice would drive a ~0.7 psu salinization over a ~50 m water column typical of the region, a salinity change that is in reasonable agreement with the ~1 psu seasonal change in salinity estimated from 14 years of mooring measurements (Woodgate et al., 2005a).

Combining ice thickness data with ice velocity data, Travers (2012) estimates Bering Strait sea ice to carry $\sim 140 \pm 40 \text{ km}^3$ of freshwater (relative to 34.8 psu) northward in winter 2007–2008, comparable (within errors) to the previous (crude) estimate of $\sim 100 \pm 70 \text{ km}^3 \text{ yr}^{-1}$ (Woodgate and Aagaard, 2005). Note that for the first months of the winter, the ice flux through the strait is typically southward, since northward-flowing water tends to carry no ice. Only as ice cover becomes more continuous does the net flux turn northward.

Extending this analysis to other years (author Woodgate and Cynthia Travers, unpublished data) suggests remarkably large interannual variability, with mean ice thicknesses varying from <1 m to >2 m; maximum thicknesses being over 18 m (historically, ice keels have been >20 m; Richard Moritz, University of Washington, *pers. comm.*, 2012); and northward fluxes in 2008 and 2010 being ~30% higher than in 2007, near zero in 2009, and net negative in 2011. (Here, 2007 means the winter commencing in December 2007.) These data also suggest that ice velocity is typically near zero (possibly landfast) for ~10–20% of

the ice-covered period, again with much interannual variability.

Two other quirks of Bering Strait sea ice are worth mentioning. All of our sea ice measurements are taken in recent years, when it is hypothesized that sea ice is thinner and weaker, but in earlier decades, wintertime “ice arches” were observed in satellite imagery of the strait (in 1979, 1980, 1983, 1984, 1985), when southward-flowing ice jammed north of the strait, preventing southward ice flux through the strait and creating a polynya region south of the arch (Torgerson and Stringer, 1985; see also Kozo et al., 1987). Also, within the traditional knowledge of the region are reports of large chunks of freshwater ice (“blue ice,” good for drinking, from icebergs and/or multiyear ice) from the Arctic traversing southward through the strait (e.g., Native observations from Diomedea; Oceana and Kawarak, 2014; Raymond-Yakoubian et al., 2014). While those are observations from the past, Babb et al. (2013) track multiyear ice transiting southward from the Arctic through the strait between November 2011 and May 2012, consistent with the net southward ice flux found from the ADCP data in 2011.

Interannual Change in the Bering Strait Fluxes

So far, we have mostly confined ourselves to describing the typical physical oceanography of the strait and its seasonal variability. However, as we consider the strait’s role in climate change, a pressing question is how these processes and properties vary interannually. Various instrument and coverage issues make data sparse from the 1990s, but the time series may be considered generally as continuous from 1998 to present. In assessing the strait-scale average of water properties or sum of water fluxes, it has been found that the US mooring site A3 (often termed the “climate site”), being sited close to mid-channel ~35 km north of the strait proper at a location where the channel flows meet and combine, yields a useful average of the physical water

properties in the two channels of the strait (Woodgate et al., 2006, 2007). Data indicate that A3 temperature-salinity properties are a combination of A1 (Russian channel) and A2 (US channel) properties, and that given A2 and A3 data, it is possible to estimate A1 temperature and salinity to ~0.1°C and 0.2 psu (not shown). To obtain the total flux through the strait, it is also necessary to quantify the contributions of the ACC (obtained from mooring A4), the upper water column stratification, and sea-ice flux. Data from the recent high-resolution mooring arrays will guide details of these calibrations (author Woodgate and colleagues, unpublished data), but prior work has used standard corrections for all these terms (Woodgate et al., 2010b, 2012).

Perhaps most dramatic in the recent interannual variability is the increase in volume flux from 2001 to present day (here 2013, previously reported to 2011 [Woodgate et al., 2012], and updated in Figure 9a), an increase from ~0.7 Sv to ~1.1 Sv. Although the absolute numbers are still small, this change represents an

almost 50% increase in the flow. Since, to first order, whatever enters the Bering Strait must exit the Chukchi Sea into the Arctic Ocean, this increase has corresponding impacts, presumably increasing ventilation of the Arctic halocline and decreasing residence time of waters in the Chukchi Sea (order several months). Combined, these two effects may result in a significant change in the timing of different water properties entering the Arctic.

Coherent with this volume flux increase is change in the oceanic heat flux carried into the Chukchi/Arctic (Woodgate et al., 2010b, 2012). Since Pacific waters exit the Arctic (via the Fram Strait and the Canadian Archipelago) at near-freezing temperatures (Steele et al., 2004), we compute heat fluxes relative to -1.9°C, the freezing point of Bering Strait waters. This allows us to quantify the heat lost from the Pacific waters somewhere in the Chukchi/Arctic system. Including corrections for the ACC and stratification, calendar-mean Bering Strait heat fluxes (Figure 9d) are ~3–6 × 10²⁰ J yr⁻¹ (i.e., 10–20 TW; Woodgate et al., 2010b),

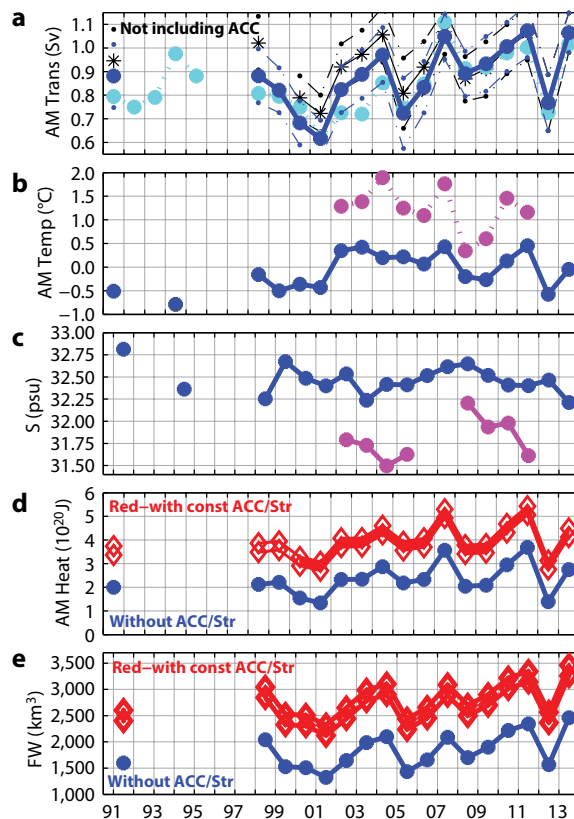


FIGURE 9. Bering Strait annual mean time series from 1991–2013 of: (a) transport calculated from A3 (blue) or A2 (cyan), adjusted for changes in instrument depth (black) with error bars (dashed) calculated from variability; (b) near-bottom temperatures from A3 (blue) and A4 (magenta-dashed); (c) salinities from A3 (blue) and A4 (magenta); (d) heat fluxes (relative to -1.9°C): blue – from A3 only; red – including constant corrections for ACC (1×10^{20} J) and stratification (0.4 to 1.7×10^{20} J), latter estimates taken from average correction for a 10 m or 20 m thick upper layer in Woodgate et al., (2012); and (e) freshwater fluxes (relative to 34.8 psu): blue – from A3 only; red – including 800–1,000 km³ (lower and upper bounds) correction for stratification and ACC. Updated from Woodgate et al. (2012); see that paper for full methodology.

comparable to the shortwave solar input to the Chukchi Sea (Perovich et al., 2007), and about one-third of the Fram Strait heat flux (Schauer et al., 2008). Although undoubtedly some heat is lost in transit through the Chukchi Sea (Woodgate et al., 2005b), this quantity of heat is sufficient to melt $1\text{--}2 \times 10^6 \text{ km}^2$ of 1 m thick ice, an area equivalent to one-third to one-fifth of annual Arctic sea-ice retreat (Woodgate et al., 2010b). While several other factors contribute to Arctic sea-ice loss (especially the ice albedo feedback), those authors hypothesize that the Bering Strait heat flux acts as a trigger to create open water upon which the ice-albedo feedback can act, and also provides a year-round subsurface source of heat potentially thinning Arctic sea ice, since Pacific summer waters are found throughout roughly half of the Arctic Ocean (Steele et al., 2004).

Pacific waters contribute approximately one-third of the freshwater entering the Arctic Ocean (Aagaard and Carmack, 1989; Serreze et al., 2006). As per these authors, we calculate freshwater fluxes relative to 34.8 psu, an estimate of the mean salinity of the Arctic, and thus our flux is an estimate of the ability of the inflow to freshen the Arctic Ocean. Woodgate et al. (2012) documented freshwater flux increases from 2,000–2,500 km^3 in 2001 to 3,000–3,500 km^3 in 2011. That increase is almost twice the interannual variability found in other freshwater sources to the Arctic (i.e., river run off variability of $\sim 400 \text{ km}^3 \text{ yr}^{-1}$, Shiklomanov and Lammers, 2009; and precipitation-evaporation variability of $\sim 500 \text{ km}^3 \text{ yr}^{-1}$, Serreze et al., 2006). Our extended freshwater flux time series (Figure 9e) shows that, although 2012 had a low freshwater flux, the 2013 flux equaled the record maximum of $\sim 3,500 \text{ km}^3$, the increase being in part due to falling salinities.

In addition to net flux properties, local conditions are also changing, with lower layer temperatures (but not sea surface temperatures) being warmer in recent years, and warmer waters

arriving $1.6 \pm 1.1 \text{ days yr}^{-1}$ earlier in the strait, resulting in a longer warm season (Woodgate et al., 2012). As discussed above, there is also large interannual variability in sea-ice fluxes (author Woodgate and Cynthia Travers, unpublished data).

Teasing apart the mechanisms for these changes is nontrivial. Prior work (Woodgate et al., 2012) suggests that $\sim 50\%$ of the heat flux and $\sim 90\%$ of the freshwater flux changes are due to changes in the volume flux, and that, in turn, approximately one-third of the volume flux change is associated with changes in the local wind, while the remaining two-thirds is likely due to the far-field forcing of the flow, believed to be related to a Pacific-Arctic pressure difference (for a discussion of Bering Strait forcings, see, e.g., Woodgate et al., 2005b). More recent work (Danielson et al., 2014) links the far-field forcing of the flow to the position of the atmospheric Aleutian Low pressure system. There are some indications that the earlier warming in spring relates to faster transport of waters from the Bering Sea (Woodgate et al., 2012), but there is still no clear understanding of how Bering Sea water properties may affect the properties in the strait. Establishing mechanistic or statistical linkages may require a skilled model of the region (e.g., Nguyen et al., 2012). However, given the comparatively poor linkages between remotely sensed data (e.g., wind and SST) and the fluxes through the strait, in situ moorings still remain the only reliable method of quantifying the Bering Strait throughflow.

THE BIOGEOCHEMICAL OCEANOGRAPHY OF THE BERING STRAIT

Biogeochemical studies of the Bering Strait are far less advanced than physical oceanographic studies since, until about the year 2000, biogeochemical measurements were primarily made only from water samples gathered from ships and were thus sparse in space and time. Nonetheless, ship-based station data (e.g., Walsh et al., 1989; Cooper

et al., 1997) established the existence of strong cross-strait and vertical gradients in biogeochemical properties, with, for example, nutrients being low in surface waters (especially in the eastern channel) and near the US coast in the ACW. The nutrient-rich waters of the Russian channel were related to waters passing through the Gulf of Anadyr on the Russian coast at $\sim 64^\circ\text{N}$, and these waters are often called Anadyr Waters. In a pilot study to obtain time-series measurements, from July to September 2001 and from March to May 2003 a laboratory based on Little Diomed Island sampled water (from $\sim 5 \text{ m}$ depth) pumped ashore via a pipe extending 120 m offshore into the channel between Little and Big Diomed Islands (Cooper et al., 2006). However, logistical and scientific issues remained to be solved with this approach, with measurements being strongly influenced by wind, vulnerable to runoff from the island, and likely biased due to the trapped island circulations described above. Instead, some progress has been made with mooring technologies that allow (at least in design) for year-round automated measurements.

Nutrients and Bio-Optics: Nitrate, Fluorescence, and Turbidity

Various automated nitrate samplers have been deployed in the strait since 2000 (Table 1; Terry Whitledge, University of Alaska Fairbanks, unpublished data). The earliest of these, the NAS Nutrient Analyzer instrument, employed wet chemistry techniques, with bags of reagents included in the instrument. However, deployments from 2000 to 2003 demonstrated this design was insufficiently robust to work in the challengingly cold, high-flow waters of the strait.

Far greater success has been achieved with the optical ISUS, deployed annually in the strait at two mooring sites since 2005. While data calibration still has to be completed (especially since the ISUS appears to be sensitive to drift; Phyllis Stabeno, NOAA, *pers. comm.*, 2013), year-long time series indicate significant

seasonal change in the nitrate levels in the strait, ranging from 8–32 μM over the course of a year in data from the near coastal mooring in the Russian channel (A1W) (Weingartner and Whitlege, 2013; Whitlege and Stockwell, 2013). These authors show a strong positive correlation exists between nitrate and independent salinity measurements, probably reflecting that the nutrient-rich Anadyr Waters are also comparatively salty. As for salinity, measured nitrate levels vary widely and rapidly as water temperatures fall in autumn, likely due to the mixing down (discussed above) of nutrient-depleted (fresher) surface waters to the ~30–40 m depth of the instrument. Their data suggest an increase of nutrients in winter, often followed by a spring depletion, which we suggest may be driven by the spring bloom (when it is coincident with peaks in fluorescence, see below). Summer section data (Lee et al., 2007) raise the possibility of significant (~30%) reduction in nutrients in the strait from 2002 to 2004, although those authors admit this apparent change may be due to the large spatial and temporal variations in the region rather than interannual variability. Analysis of the fully calibrated in situ multiyear ISUS data should cast some light on this issue, as well as elucidate the seasonal cycle.

Similarly, bio-optical instruments, deployed since 2002, allow an assessment of the seasonality of fluorescence and turbidity (Terry Whitlege and Thomas Weingartner, University of Alaska Fairbanks, unpublished data). Calibrations (ongoing) are particularly challenging due to biofouling, although the use of copper foil and bio-wiper instruments have decreased this problem. Preliminary data plots (in Whitlege and Stockwell, 2013, and in cruise reports at <http://psc.apl.washington.edu/BeringStrait.html>) typically show that chlorophyll (as measured by fluorescence) is very low in winter, but starts to increase at roughly the same time as the strait starts to melt out and freshen. It is notable this increase seems to occur under sea ice,

coincident with the seasonal onset of solar shortwave radiation reaching the water as sea-ice concentration starts to fall (data as per Perovich et al., 2007) and often starts to thin (author Woodgate and Cynthia Travers, unpublished data). A more rapid rise in fluorescence occurs as water temperatures start to warm, likely with the onset of the spring bloom. In most of the records, the spring bloom yields the highest chlorophyll signals, with fluorescence being lower during the rest of the summer and autumn. In contrast, one record, that from the ACC site A4 in 2010 (Woodgate and the RUSALCA 2011 Science Team, 2011), shows also a weaker but significant autumn bloom, although this is not reproduced in the A4 record in 2011, the only other year for which we have data at this location. The fluorescence signals are often

site A4 (Woodgate and the RUSALCA 2011 Science Team, 2011; Woodgate and the RUSALCA 2012 Science Team, 2012), likely due to sediment of coastal origin carried by the ACC.

Ocean Acidification

Even more recently, preliminary efforts have been made to establish year-round measurements of $p\text{CO}_2$ and pH in the strait for purposes of studying ocean acidification (author Prahl, unpublished data, available at <http://www.aoncadis.org>). While the entire Arctic Ocean is thought to represent 5–14% of the global ocean sink for atmospheric carbon dioxide (see, e.g., Bates and Mathis, 2009, and references therein), increased atmospheric CO_2 levels, decreasing sea-ice coverage, and increasing freshwater

“While we are slowly overcoming the technical challenges of chemical and biogeochemical measurements in these cold, biofouling environments, we still lack an appreciation of seasonal and interannual variability and, importantly, the fundamental understanding of the length scales and time scales of the variability in these parameters that is required to make sense of necessarily sparse observations.”

episodic, but it must be remembered that, due to ice-keel risk, these instruments are deployed at ~40–50 m depth, and thus are likely often measuring the fallout of the bloom, rather than the bloom itself. Times of high fluorescence often correspond with times of high turbidity, although high turbidity signals are also found without corresponding elevated fluorescence, the most notable example being the winter-long high turbidity signals found at

input are likely increasing Arctic CO_2 uptake. These changes are making Arctic waters increasingly corrosive to the calcareous shells of marine taxa, which frequently are at the bottom of the Arctic food chain (for review, see Fabry et al., 2009). Thus, assessing this acidification in the rich marine ecosystems of the Bering and Chukchi Seas is particularly important. Again, the Bering Strait provides a spatially manageable and critical point

for assessing these changes.

In a “proof-of-concept” project, pH, $p\text{CO}_2$, and dissolved oxygen (DO) sensors were deployed on mooring A3 (the climate mooring) from 2011–2012, and 2012–2013. Data return (Table 1) was somewhat compromised by various instrument issues, provoked by the cold,

Science Team, 2012). ($\Omega_{\text{aragonite}} < 1$ indicates dissolution of calcium carbonate is favored; see, e.g., Bates and Mathis, 2009, for discussion.) On July 14, 2012, $\Omega_{\text{aragonite}}$ was everywhere greater than 1, with highest values ($\sim 2\text{--}3$) being found in the surface layer in the center of the channel, while the bottom waters in the

et al., 2011). Overall, these measurements suggest that the region is not currently corrosive to aragonite, although the low $\Omega_{\text{aragonite}}$ values near the coast suggest future vulnerability, especially in light of the increased freshening trend observed (which tends to lower $\Omega_{\text{aragonite}}$ values).

In August 2005, Chierici and Fransson (2009) found similar $\Omega_{\text{aragonite}}$ values near the Alaskan coast and in the surface of the strait, but with little stratification in the strait, so that the $\Omega_{\text{aragonite}}$ in bottom water was ~ 2 . Data from 2002 and 2004 in Bates et al. (2009), although not explicitly discussed by those authors, show little or no vertical gradient in spring (early/mid May, $\Omega_{\text{aragonite}} \sim 1.5$ [2002], 1.8–2.5 [2004] in both surface and bottom waters), but some stratification in summer (mid-July, $\Omega_{\text{aragonite}} \sim 3$ [surface] to 2 [bottom], both years). Our inability to determine if these differences are seasonal or inter-annual indicates the driving necessity for time-series measurements in the strait.

Lacking $p\text{CO}_2$ measurements, we are unable to calculate $\Omega_{\text{aragonite}}$ from the mooring pH data we acquired, but, since high pH generally favors high $\Omega_{\text{aragonite}}$ (and vice versa), we can investigate pH changes to obtain at least a first-order indication of the temporal dynamics of the oceanic carbonate system in these waters. Our July section data (2011 and 2012) show pH varies spatially similarly to $\Omega_{\text{aragonite}}$ —in these years, the lower layer US channel waters have pH ~ 8.15 , often slightly higher at the surface ($\sim 8.3\text{--}8.5$ pH units), while the waters on the Alaskan coast have slightly lower (more acidic) values (pH $\sim 8\text{--}8.15$), with values increasing at depth (Woodgate and the RUSALCA 2012 Science Team, 2012). Again, rerunning the sections within a few days shows small but significant changes, order 0.05 to 0.1 pH units.

At ~ 48 m depth on mooring A3, the one year of pH mooring data (July 2011–July 2012, with end points within ~ 0.1 pH of bottle sample data; Woodgate and the RUSALCA 2012 Science Team, 2012) show significant episodic variability (from 8–8.3 pH units) in summer and

“As the predictions of the climate models are for enhanced change in the Bering Strait [and] as Native science and Western science both document unexpectedly large changes in the ecosystems in recent years...we must act rapidly to establish at least a baseline, fundamental understanding of the fully coupled biogeochemical and ecological system in the Pacific Gateway to the Arctic.”

biofouling environment. However, in total, we obtained one month of SAMI (Submersible Autonomous Moored Instrument) pH data from Sunburst Sensors in summer 2011 and one year of pH data from the only deployment of the SeapHox instrument (a field effect transistor system developed by Todd Martz, Scripps Institution of Oceanography), also in summer 2011 (Woodgate and the RUSALCA 2012 Science Team, 2012; Woodgate and the Bering Strait 2013 Science Team, 2013). To provide a spatial context, water samples were also taken by a CTD rosette for $p\text{CO}_2$, dissolved inorganic carbon, and total alkalinity determinations from sections in the US channel and through the mooring site A3 in July 2011, 2012, and 2013.

Data from these water samples allow us to draw low spatial resolution sections of the aragonite saturation state ($\Omega_{\text{aragonite}}$) in the US channel of the strait (Woodgate and the RUSALCA 2012

channel had lower values, $\Omega_{\text{aragonite}} \sim 1.3$. By the Alaskan coast, surface waters had intermediate $\Omega_{\text{aragonite}}$ values (~ 1.7), with some indication of $\Omega_{\text{aragonite}}$ increasing slightly with depth. A repeat of the section on July 19, 2012, just five days later, shows some values (near the center of the channel) changed by ~ 0.5 , but patterns remain the same. Indeed, the same pattern was found in July 2011 and 2013. We hypothesize that the strong vertical gradient in $\Omega_{\text{aragonite}}$ in the strait is due to upper water column primary production increasing saturation state near the surface (due to biological uptake of CO_2 in the water) and decreasing saturation state at depth (due to aerobic remineralization of the primary production as it sinks), processes described in Bates et al. (2009). Meanwhile, the comparatively low values of $\Omega_{\text{aragonite}}$ near the Alaskan coast likely relate to the modifying chemical influence of riverine waters, as noted further south in the Bering Sea (Mathis

fall. While winter pH values are more uniform (around 8.1), the episodic increases in pH signal return as the waters start to warm after the winter (as discussed above), likely linked with the onset of the spring bloom. Such variability may possibly be due to biological uptake of CO₂ even at these depths, since, as discussed above, during this initial warming, the water column may be mixed from ~15 m depth to the bottom, and the ISUS nutrient data from the same depth (albeit at a different mooring location) also show nitrate drawdown coincident with the spring bloom. However, the pH changes could also reflect advection of waters from the south. The one month of SAMI data (July–August 2011) show pH to be strongly correlated with ISUS nitrate and (at some times, seemingly when the mooring is dominated by Russian channel waters) also strongly correlated with temperature, with pH being lower in the high-nitrate, colder waters typical of the Anadyr Waters (preliminary data in Woodgate and the RUSALCA 2012 Science Team, 2012).

Some oxygen data were also recovered from these deployments—six months from the SAMI pH, one year from the SeapHox. However, the records are dissimilar and, in the absence of collaborating bottle data, we neglect them here, noting only that both records suggest times of oxygen supersaturation caused by net primary production, as is found in section data (see above).

While the results relevant to ocean acidification are preliminary and the data set is sparse, they are sufficient to demonstrate the high temporal and spatial variability of the biogeochemistry in the Bering Strait. Our findings also illustrate the dangers inherent to inferring interannual change from section data alone. To understand (and thus predict) the regional biogeochemistry (and also its far-field influence) will require year-round measurements and a much greater understanding of the spatial and temporal variability in the narrow yet complex gateway between the Pacific and Arctic Oceans.

MOORED MARINE MAMMAL OBSERVATIONS IN THE BERING STRAIT

As discussed earlier, recent years show increases in heat and freshwater fluxes and the open water season in the Bering Strait region. The biological responses to these physical changes are complex but may result in a shift in the northern Bering Sea and Bering Strait from an Arctic-type ecosystem to a sub-Arctic type ecosystem (Grebmeier et al., 2006b; Grebmeier, 2012). One way to monitor changes in, or impacts on, an ecosystem is to observe the response of a suite of upper trophic level species such as seabirds and marine mammals via changes in occurrence and/or distribution (Moore et al., 2014). For instance, the Pacific Arctic Region ecosystem “reorganization,” from benthic- to pelagic-based (possibly linked to sea-ice decline; e.g., Hunt et al., 2002), and sea-ice decline itself, might negatively impact marine mammal species that rely on sea ice for habitat (e.g., ice seals, walrus, bowhead whales) and/or benthic infauna for food (e.g., walrus, gray whales, some ice seals) via a reduction in habitat and prey abundance (Grebmeier et al., 2006a). Other species, however, such as sub-Arctic “summer whales” may benefit from increased access to northern habitat and pelagic prey species (Moore and Huntington, 2008; Clarke et al., 2013a). While the risk of potential competition for resources from sub-Arctic species expanding northward is poorly understood (Clarke et al., 2013a), integrating upper trophic level species with environmental data can provide insight into those environmental drivers that might result in increased competition. Furthermore, assessment of the impacts of increased human activities in the Arctic (such as marine resource extraction and increased shipping) requires improved basic marine mammal population information (Reeves et al., 2014). Finally, there is concern among Native Alaskans who live in the villages of the Arctic that environmental changes may result in changes in distribution of, and access to, species that

are important for subsistence.

The southern Chukchi Sea/Bering Strait region is the gateway for Arctic marine mammals such as the bowhead whale that winter in the Bering Sea and summer in the Pacific Arctic. Sub-Arctic species, including fin, humpback, and killer whales, occurred here historically and are being seen with increasing frequency by aerial and shipboard surveys (Clarke et al., 2013a). Whether these species are re-occupying old habitat or exploiting new habitat provided by decreased seasonal sea ice is unknown. Changes in marine mammal occurrence can be detected both visually (during cruises with visual survey effort) and acoustically by recording underwater sounds made by marine animals, ships, and ice and wind. Traditional visual survey methods are hampered by poor weather, ice cover, and limited daylight hours. The use of passive acoustic monitoring overcomes these constraints and permits the detection of vocally active species.

Beginning in 2009, hydrophone packages were added to the mooring at A3. These instruments sampled at 8,192 Hz on a duty cycle of 10 min hr⁻¹. Spectrograms showing time, frequency, and amplitude of each acoustic data file were generated and the presence (1) or absence (0) of at least one species-specific call was noted for each hour for fin, humpback, killer, and bowhead whales. In the shallow Chukchi Sea, we likely detect all calls within 10 to 20 km, and perhaps some up to 30 km away.

From September to December of every year from 2009 to 2012 (Figure 10), in addition to the Arctic bowhead whale, we also recorded the sub-Arctic species humpback, fin, and killer whales. Humpback whales were detected from September through October, most often in 2009 and 2012, with fewer hours with calls in 2010 and 2011. Fin whales were recorded most commonly in 2012 followed by 2009, with fewer calls being detected in 2010 and 2011. Killer whales were the third most commonly recorded

sub-Arctic species and were recorded sporadically in all four years but most frequently in 2012. Photographs of killer whales in the Chukchi Sea and acoustic data indicate that the whales that are found in the Chukchi Sea are of the mamm-eating ecotype and are likely following other sub-Arctic species, including gray whales, north in the summer as seasonal sea ice retreats (Higdon and Ferguson, 2009; Ferguson et al., 2010). Detections of these sub-Arctic cetaceans all ended in late October/early November, before the formation of seasonal sea ice. Figure 10 shows the distribution of all whale calls by year with also the corresponding temperature-salinity properties in the strait. Oceanographic conditions in both 2009 and 2012 (the high-call years for sub-Arctic species) were characterized by colder, saltier water, possibly indicating the greater presence of nutrient-rich Anadyr Water at this site in these years (similar to Russell et al., 1999, in the Bering Sea). The interannual variability in the presence of sub-Arctic whales,

also documented by acoustic and visual survey data (Clarke et al., 2013a), may be related to this temperature-salinity variability. For example, in the southern Chukchi Sea, greater abundances of large zooplankton and forage fish, which are known prey of fin and humpback whales, are found in cooler, higher nutrient waters (Eisner et al., 2013).

Bowhead whales migrate south through the Bering Strait in early winter after feeding in the eastern Beaufort Sea and near the Russian Chukchi coast all summer and fall (Quakenbush et al., 2010). Thus, the Bering Strait region is part of the winter range of bowhead whales (Citta et al., 2012), and that is reflected in the occurrence of bowhead signals nearly every hour beginning in mid-November (Figure 10). Bowhead whale calls did not show the same interannual variability as the sub-Arctic species' calls, although bowhead whales were recorded earliest in the year and most often in 2012, a year when the velocity data (not shown) suggest

anomalously southward flow commencing in mid-October, shortly before onset of continuous bowhead calls. Note that aerial survey data from the northeastern Chukchi Sea also found many more bowheads than usual in September and October 2012 (Clarke et al., 2013b).

The seasonal presence of sub-Arctic cetaceans in the Bering Strait region is certainly due to foraging opportunities, with resource availability enhanced by the decrease in seasonal sea ice (i.e., increased habitat) and post-whaling population increases. This increased presence could result in competition for resources with Arctic marine mammals such as bowhead whales, particularly if these species overlap more in space and time than at present. The Pacific Arctic is currently experiencing ecosystem shifts over multiple trophic levels (Grebmeier, 2012). Marine mammals are sentinels of Arctic ecosystem changes (Moore et al., 2014), and understanding the physical drivers of these shifts, and how they vary over annual,

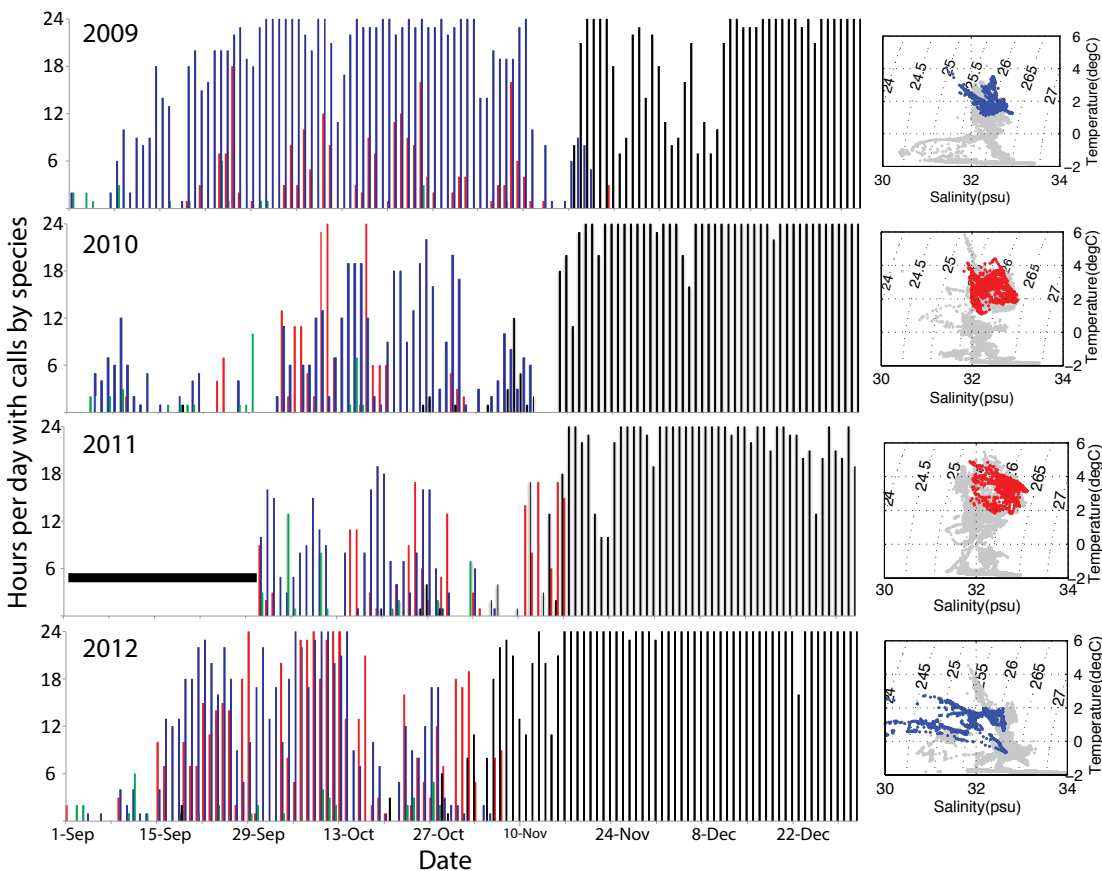


FIGURE 10. Hours per day with acoustic detections of humpback (blue bars), fin (red bars), killer (green bars), and bowhead (black bars) whales at mooring A3 in the Bering Strait from September through December for years 2009 to 2012 (excepting September 2011, when no data were available). Temperature-salinity data for each year are shown in the right-hand column with values for September and October of each year shown as blue (cold years) or red (warm years) dots.

decadal, and longer time scales, requires long-term monitoring of their presence within the ecosystem.

DIRECTIONS FOR THE FUTURE

What lessons can we learn from this prior work as we look toward research and measurement goals for the Bering Strait for the future? We are struck immediately with two distinct but related challenges. The first is how to efficiently quantify those important properties of the throughflow that we already mostly understand. The second is how to address the important gaps in our understanding of the daily, seasonal, interannual, and spatial changes of the complete interdisciplinary system of the strait region.

As outlined above, by far the most progress has been made in the physical oceanography of the strait. Past measurements have provided a fair understanding of the relevant spatial and temporal scales that we must capture to properly describe the physical system of the strait, and have established that a reasonable quantification of water properties and fluxes of volume, heat, and freshwater may be obtained from three moorings in US waters (A2, A3, and A4). In an ongoing NSF-AON project, these measurements will be combined with Native knowledge, high-resolution ocean modeling, and continued summer hydrographic measurements to ascertain previously overlooked features and provide a longer-time perspective for the time series (author Rebecca Woodgate, APL; Patrick Heimbach and An Nguyen, MIT; Julie Raymond-Yakoubian, Kawerak, Inc., *pers. comm.*, 2012).


Yet, while a practical scheme exists for these measurements, there are still urgent gaps in our physical knowledge of the strait, most notably in our understanding of the driving mechanisms (especially the far field driving) both of the main flow and of the boundary currents, and the disciplinary and interdisciplinary impacts of the smaller-scale features, such as eddies, and topography (island)-driven mixing. Advances here will likely

require a combination of observations, theory, and modeling.

Even greater unknowns exist in the biogeochemical and ecosystem realm. It is obvious from the results presented above that these measurements are still very much in their infancy. While we are slowly overcoming the technical challenges of chemical and biogeochemical measurements in these cold, biofouling environments, we still lack an appreciation of seasonal and interannual variability and, importantly, the fundamental understanding of the length scales and time scales of the variability in these parameters that is required to make sense of necessarily sparse observations. Furthermore, understanding of results higher up the ecosystem will rely on our ability to characterize the basic biogeochemistry of the strait. Year-round time-series measurements, to provide a short-time-scale and seasonal/interannual understanding of variability, will be a vital part of solving these puzzles. As the physical oceanography shows, the strait is subject to dramatic change on short time and space scales, and it is essential to take this variability into account when interpreting data.

Finally, inherent to all these biogeochemical questions is the necessity for a “whole strait” understanding, including both the nutrient-rich waters in the Russian channel and the nutrient-poor waters of the US channel.

Over the 25 years since the mooring program in the Bering Strait was established, great progress has been made measuring a system that was initially (naively) assumed to be interannually comparatively static. As the predictions of the climate models are for enhanced change in the Bering Strait (e.g., Holland et al., 2007), as Native science and Western science both document unexpectedly large changes in the ecosystems in recent years (Grebmeier, 2012; Oceana and Kawerak Inc., 2014), and as increased commercial pressure make comprehension of the region more necessary for environmental protection (e.g., Reeves et al., 2014),

we must act rapidly to establish at least a baseline, fundamental understanding of the fully coupled biogeochemical and ecological system in the Pacific Gateway to the Arctic. 

REFERENCES

- Aagaard, K., and E.C. Carmack. 1989. The role of sea ice and other fresh water in the Arctic circulation. *Journal of Geophysical Research* 94(C10):14,485–14,498, <http://dx.doi.org/10.1029/JC094iC10p14485>.
- Ahlnäs, K., and G.R. Garrison. 1984. Satellite and oceanographic observations of the warm coastal current in the Chukchi Sea. *Arctic* 37:244–254, <http://dx.doi.org/10.14430/arctic2197>.
- Babb, D.G., R.J. Galley, M.G. Asplin, J.V. Lukovich, and D.G. Barber. 2013. Multiyear sea ice export through the Bering Strait during winter 2011–2012. *Journal of Geophysical Research* 118(10):5,489–5,503, <http://dx.doi.org/10.1002/jgrc.20383>.
- Bates, N.R., and J.T. Mathis. 2009. The Arctic Ocean marine carbon cycle: Evaluation of air-sea CO₂ exchanges, ocean acidification impacts and potential feedbacks. *Biogeosciences* 6(11):2,433–2,459, <http://dx.doi.org/10.5194/bg-6-2433-2009>.
- Bates, N.R., J.T. Mathis, and L.W. Cooper. 2009. Ocean acidification and biologically induced seasonality of carbonate mineral saturation states in the western Arctic Ocean. *Journal of Geophysical Research* 114, C11007, <http://dx.doi.org/10.1029/2008jc004862>.
- Bell, J., J. Betts, and E. Boyle. 2002. MITESS: A moored in situ trace element serial sampler for deep-sea moorings. *Deep Sea Research Part I* 49(11):2,103–2,118, [http://dx.doi.org/10.1016/S0967-0637\(02\)00126-7](http://dx.doi.org/10.1016/S0967-0637(02)00126-7).
- Black, L. 2004. *Russians in Alaska, 1732–1867*. University of Alaska Press.
- Bockstoce, J.R. 1986. *Whales, Ice, and Men: The History of Whaling in the Western Arctic*. University of Washington Press.
- Brugler, E.T., R.S. Pickart, G.W.K. Moore, S. Roberts, T.J. Weingartner, and H. Statscewich. 2014. Seasonal to interannual variability of the Pacific water boundary current in the Beaufort Sea. *Progress in Oceanography* 127:1–20, <http://dx.doi.org/10.1016/j.poccean.2014.05.002>.
- Chierici, M., and A. Fransson. 2009. Calcium carbonate saturation in the surface water of the Arctic Ocean: Undersaturation in freshwater influenced shelves. *Biogeosciences* 6(11):2,421–2,431, <http://dx.doi.org/10.5194/bg-6-2421-2009>.
- Citta, J.J., L.T. Quakenbush, J.C. George, R.J. Small, M.P. Heide-Jørgensen, H. Brower, B. Adams, and L. Brower. 2012. Winter movements of bowhead whales (*Balaena mysticetus*) in the Bering Sea. *Arctic* 65:13–34, <http://dx.doi.org/10.14430/arctic4162>.
- Clarke, J.T., A.A. Brower, C.L. Christman, and M.C. Ferguson. 2013b. *Distribution and Relative Abundance of Marine Mammals in the Northeastern Chukchi and Western Beaufort Seas, 2012*. National Marine Mammal Laboratory, Alaska Fisheries Science Center, NMFS, NOAA, 364 pp.
- Clarke, J., K. Stafford, S.E. Moore, B. Rone, L. Aerts, and J. Crance. 2013a. Subarctic cetaceans in the southern Chukchi Sea: Evidence of recovery or response to a changing ecosystem. *Oceanography* 26(4):136–149, <http://dx.doi.org/10.5670/oceanog.2013.81>.
- Coachman, L.K., and K. Aagaard. 1966. On the water exchange through Bering Strait. *Limnology and Oceanography* 11(1):44–59, <http://dx.doi.org/10.4319/lo.1966.11.1.0044>.
- Coachman, L.K., K. Aagaard, and R.B. Tripp. 1975. *Bering Strait: The Regional Physical Oceanography*. University of Washington Press, Seattle, 172 pp.

- Cooper, L.W., L.A. Codispoti, V. Kelly, G.G. Sheffield, and J.M. Grebmeier. 2006. The potential for using Little Diomedede Island as a platform for observing environmental conditions in Bering Strait. *Arctic* 59(2):129–141, <http://dx.doi.org/10.14430/arctic336>.
- Cooper, L.W., T.E. Whittedge, J.M. Grebmeier, and T. Weingartner. 1997. The nutrient, salinity, and stable oxygen isotope composition of Bering and Chukchi Seas waters in and near the Bering Strait. *Journal of Geophysical Research* 102(C6):12,563–12,573, <http://dx.doi.org/10.1029/97JC00015>.
- Danielson, S.L., T.J. Weingartner, K.S. Hedstrom, K. Aagaard, R. Woodgate, E. Curchitser, and P.J. Stabenro. 2014. Coupled wind-forced controls of the Bering–Chukchi shelf circulation and the Bering Strait throughflow: Ekman transport, continental shelf waves, and variations of the Pacific–Arctic sea surface height gradient. *Progress in Oceanography* 125:40–61, <http://dx.doi.org/10.1016/j.pocean.2014.04.006>.
- De Boer, A.M., and D. Nof. 2004. The Bering Strait's grip on the northern hemisphere climate. *Deep Sea Research Part I* 51(10):1,347–1,366, <http://dx.doi.org/10.1016/j.dsr.2004.05.003>.
- Dyke, A.S., J.E. Dale, and R.N. McNeely. 1996. Marine molluscs as indicators of environmental change in glaciated North America and Greenland during the last 18,000 years. *Géographie Physique et Quaternaire* 50(2):125–184, <http://dx.doi.org/10.7202/033087ar>.
- Eisner, L., N. Hillgruber, E. Martinson, and J. Maselko. 2013. Pelagic fish and zooplankton species assemblages in relation to water mass characteristics in the northern Bering and southeast Chukchi Seas. *Polar Biology* 36(1):87–113, <http://dx.doi.org/10.1007/s00300-012-1241-0>.
- Fabry, V.J., J.B. McClintock, J.T. Mathis, and J.M. Grebmeier. 2009. Ocean acidification at high latitudes: The bellwether. *Oceanography* 22(4):160–171, <http://dx.doi.org/10.5670/oceanog.2009.105>.
- Ferguson, S., J. Higdon, and E. Chmelitskiy. 2010. The rise of killer whales as a major Arctic predator. Pp. 117–136 in *A Little Less Arctic: Top Predators in the World's Largest Northern Inland Sea*, Hudson Bay. S.H. Ferguson, L.L. Loseto, and M.L. Mallory, eds, Springer.
- Fitzhugh, B. In press. Origins and development of Arctic maritime adaptations in the western subarctic. In *Oxford Handbook on Arctic Archaeology*. T.M. Friesen and O.K. Mason, eds, Oxford University Press, Oxford.
- Francis, J.A., E. Hunter, J.R. Key, and X. Wang. 2005. Clues to variability in Arctic minimum sea ice extent. *Geophysical Research Letters* 32, L21501, <http://dx.doi.org/10.1029/2005GL024376>.
- Grebmeier, J.M. 2012. Shifting patterns of life in the Pacific Arctic and sub-Arctic Seas. *Annual Review of Marine Science* 4(1):63–78, <http://dx.doi.org/10.1146/annurev-marine-120710-100926>.
- Grebmeier, J.M., L.W. Cooper, H.M. Feder, and B.I. Sirenko. 2006a. Ecosystem dynamics of the Pacific-influenced northern Bering and Chukchi Seas in the Amerasian Arctic. *Progress in Oceanography* 71:331–361, <http://dx.doi.org/10.1016/j.pocean.2006.10.001>.
- Grebmeier, J.M., J.E. Overland, S.E. Moore, E.V. Farley, E.C. Carmack, L.W. Cooper, K.E. Frey, J.H. Helle, F.A. McLaughlin, and S.L. McNutt. 2006b. A major ecosystem shift in the northern Bering Sea. *Science* 311:1,461–1,464, <http://dx.doi.org/10.1126/science.1121365>.
- Gudkovich, Z.M. 1962. On the nature of the Pacific current in Bering Strait and the causes of its seasonal variations. *Deep Sea Research* 9:507–510, Translated from the Russian journal *Okeanologiya* 1961 1(4):1,608–1,612, [http://dx.doi.org/10.1016/0011-7471\(62\)90103-1](http://dx.doi.org/10.1016/0011-7471(62)90103-1).
- Hasegawa, D., M.R. Lewis, and A. Gangopadhyay. 2009. How islands cause phytoplankton to bloom in their wakes. *Geophysical Research Letters* 36, L20605, <http://dx.doi.org/10.1029/2009GL039743>.
- Higdon, J.W., and S.H. Ferguson. 2009. Loss of Arctic sea ice causing punctuated change in sightings of killer whales (*Orcinus orca*) over the past century. *Ecological Applications* 19(5):1,365–1,375, <http://dx.doi.org/10.1890/07-1941.1>.
- Hoffecker, J.F., and S.A. Elias. 2003. Environment and archeology in Beringia. *Evolutionary Anthropology: Issues, News, and Reviews* 12(1):34–49, <http://dx.doi.org/10.1002/evan.10103>.
- Holland, M.M., J. Finnis, A.P. Barrett, and M.C. Serreze. 2007. Projected changes in Arctic Ocean freshwater budgets. *Journal of Geophysical Research* 112, G04S55, <http://dx.doi.org/10.1029/2006JG000354>.
- Hu, A.X., G.A. Meehl, and W.Q. Han. 2007. Role of the Bering Strait in the thermohaline circulation and abrupt climate change. *Geophysical Research Letters* 34, L05704, <http://dx.doi.org/10.1029/2006GL028906>.
- Hunt, G.L., P. Stabenro, G. Walters, E. Sinclair, R.D. Brodeur, J.M. Napp, and N.A. Bond. 2002. Climate change and control of the southeastern Bering Sea pelagic ecosystem. *Deep Sea Research Part II* 49(26):5,821–5,853, [http://dx.doi.org/10.1016/S0967-0645\(02\)00321-1](http://dx.doi.org/10.1016/S0967-0645(02)00321-1).
- Jackson, J.M., S.E. Allen, F.A. McLaughlin, R.A. Woodgate, and E.C. Carmack. 2011. Changes to the near-surface waters in the Canada Basin, Arctic Ocean from 1993–2009: A basin in transition. *Journal of Geophysical Research* 116, C10008, <http://dx.doi.org/10.1029/2011jc007069>.
- Jakobsson, M., C. Norman, J. Woodward, R. MacNab, and B. Coakley. 2000. New grid of Arctic bathymetry aids scientists and map makers. *Eos Transactions, American Geophysical Union* 81(9), 89, 93, 96, <http://dx.doi.org/10.1029/00EO00059>.
- Jones, E.P., and L.G. Anderson. 1986. On the origin of the chemical properties of the Arctic Ocean halocline. *Journal of Geophysical Research* 91(C9):759–767, <http://dx.doi.org/10.1029/JC091C09p10759>.
- Jones, E.P., J.H. Swift, L.G. Anderson, M. Lipizer, G. Civitarese, K.K. Falkner, G. Kattner, and F. McLaughlin. 2003. Tracing Pacific water in the North Atlantic Ocean. *Journal of Geophysical Research* 108(C4):13–11, <http://dx.doi.org/10.1029/2001JC001141>.
- Kozo, T.L., W.J. Stringer, and L.J. Torgerson. 1987. Mesoscale nowcasting of sea ice movement through the Bering Strait with a description of major driving forces. *Monthly Weather Review* 115(1):193–207, [http://dx.doi.org/10.1175/1520-0493\(1987\)115<0193:MNOSIM>2.0.CO;2](http://dx.doi.org/10.1175/1520-0493(1987)115<0193:MNOSIM>2.0.CO;2).
- Lavrova, O.Y., T.Y. Bocharova, and K.D. Sabinin. 2002. SAR manifestations of sea fronts and vortex streets in the Bering Strait. Pp. 2,997–2,999 in *Geoscience and Remote Sensing Symposium, 2002, IGARSS '02 IEEE International*, vol. 5. Institute of Electrical and Electronics Engineers Inc.
- Lee, S.H., T.E. Whittedge, and S.H. Kang. 2007. Recent carbon and nitrogen uptake rates of phytoplankton in Bering Strait and the Chukchi Sea. *Continental Shelf Research* 27:2,231–2,249, <http://dx.doi.org/10.1016/j.csr.2007.05.009>.
- Macdonald, R.W., T. Harner, J. Fyfe, H. Loeng, and T. Weingartner. 2003. *AMAP Assessment 2002: The Influence of Global Change on Contaminant Pathways to, within, and from the Arctic*. Arctic Monitoring and Assessment Programme (AMAP), Oslo, Norway, xii+65 pp.
- Mathis, J.T., J.N. Cross, and N.R. Bates. 2011. Coupling primary production and terrestrial runoff to ocean acidification and carbonate mineral suppression in the eastern Bering Sea. *Journal of Geophysical Research* 116, C02030, <http://dx.doi.org/10.1029/2010jc006453>.
- Moore, S.E., and H.P. Huntington. 2008. Arctic marine mammals and climate change: Impacts and resilience. *Ecological Applications* 18(sp2):S157–S165, <http://dx.doi.org/10.1890/06-0571.1>.
- Moore, S.E., E. Logerwell, L. Eisner, E.V. Farley Jr., L.A. Harwood, K. Kuletz, J. Lovvorn, J.R. Murphy, and L.T. Quakenbush. 2014. Marine fishes, birds and mammals as sentinels of ecosystem variability and reorganization in the Pacific Arctic region. Pp. 337–392 in *The Pacific Arctic Region: Ecosystem Status and Trends in a Rapidly Changing Environment*, J.M. Grebmeier and W. Maslowski, eds, Springer.
- Münchow, A., T.J. Weingartner, and L.W. Cooper. 1999. The summer hydrography and surface circulation of the East Siberian Shelf Sea. *Journal of Physical Oceanography* 29(9):2,167–2,182, [http://dx.doi.org/10.1175/1520-0485\(1999\)029<2167:tshas>2.0.co;2](http://dx.doi.org/10.1175/1520-0485(1999)029<2167:tshas>2.0.co;2).
- Nguyen, A.T., R. Kwok, and D. Menemenlis. 2012. Source and pathway of the western Arctic upper halocline in a data-constrained coupled ocean and sea ice model. *Journal of Physical Oceanography* 42(5):802–823, <http://dx.doi.org/10.1175/jpo-d-11-040.1>.
- Oceana and Kawerak Inc. 2014. *Bering Strait Marine Life and Subsistence Use Data Synthesis*. Oceana and Kawerak Inc., Juneau, AK, USA, 499 pp, <http://oceana.org/news-media/publications/reports/the-bering-strait-marine-life-and-subsistence-data-synthesis>.
- Paquette, R.G., and R.H. Bourke. 1974. Observations on the coastal current of Arctic Alaska. *Journal of Marine Research* 32(2):195–207.
- Perovich, D.K., B. Light, H. Eicken, K.F. Jones, K. Runciman, and S.V. Nghiem. 2007. Increasing solar heating of the Arctic Ocean and adjacent seas, 1979–2005: Attribution and role in the ice-albedo feedback. *Geophysical Research Letters* 34, L19505, <http://dx.doi.org/10.1029/2007GL031480>.
- Pickard, G.L., and W.J. Emery. 1990. *Descriptive Physical Oceanography: An Introduction*. Butterworth-Heinemann.
- Quakenbush, L.T., J.J. Citta, J.C. George, R.J. Small, and M.P. Heide-Jørgensen. 2010. Fall and winter movements of bowhead whales (*Balaena mysticetus*) in the Chukchi Sea and within a potential petroleum development area. *Arctic* 63:289–307, <http://dx.doi.org/10.14430/arctic1493>.
- Raymond-Yakoubian, J., Y. Khokhlov, and A. Yartzutkina. 2014. *Indigenous Knowledge and Use of Bering Strait Region Ocean Currents*. Final report to the National Park Service, Shared Beringian Heritage Program for Cooperative Agreement H9911100026, Kawerak, Inc., Social Science Program, Nome, AK, 126 pp., <http://www.kawerak.org/forms/nr/OC-report-for-web.pdf>.
- Reeves, R.R., P.J. Ewins, S. Agbayani, M.D. Heide-Jørgensen, K.M. Kovacs, C. Lydersen, R. Suydam, W. Ellliott, G. Polet, Y. van Dijk, and R. Blijleven. 2014. Distribution of endemic cetaceans in relation to hydrocarbon development and commercial shipping in a warming Arctic. *Marine Policy* 44(0):375–389, <http://dx.doi.org/10.1016/j.marpol.2013.10.005>.
- Roach, A.T., K. Aagaard, C.H. Pease, S.A. Salo, T. Weingartner, V. Pavlov, and M. Kulakov. 1995. Direct measurements of transport and water properties through the Bering Strait. *Journal of Geophysical Research* 100(C9):18,443–18,457.
- Russell, R.W., N.M. Harrison, and G.L. Hunt Jr. 1999. Foraging at a front: Hydrography, zooplankton, and avian planktivory in the northern Bering Sea. *Marine Ecology Progress Series* 182:77–93, <http://dx.doi.org/10.3354/meps182077>.
- Schauer, U., A. Beszczynska-Möller, W. Walczowski, E. Fahrba, J. Piechura, and E. Hansen. 2008. Variation of measured heat flow through the Fram Strait between 1997 and 2006. Pp. 65–85 in *Arctic-Subarctic Ocean Fluxes: Defining the Role of the Northern Seas in Climate*. R.R. Dickson, J. Meincke, and P. Rhines, eds, Springer Science.

- Serreze, M.C., A.P. Barrett, A.G. Slater, R.A. Woodgate, K. Aagaard, R.B. Lammers, M. Steele, R. Moritz, M. Meredith, and C.M. Lee. 2006. The large-scale freshwater cycle of the Arctic. *Journal of Geophysical Research* 111, C11010, <http://dx.doi.org/10.1029/2005JC003424>.
- Shiklomanov, A.I., and R.B. Lammers. 2009. Record Russian river discharge in 2007 and the limits of analysis. *Environmental Research Letters* 4, 045015, <http://dx.doi.org/10.1088/1748-9326/4/4/045015>.
- Shimada, K., T. Kamoshida, M. Itoh, S. Nishino, E. Carmack, F. McLaughlin, S. Zimmermann, and A. Proshutinsky. 2006. Pacific Ocean inflow: Influence on catastrophic reduction of sea ice cover in the Arctic Ocean. *Geophysical Research Letters* 33, L08605, <http://dx.doi.org/10.1029/2005GL025624>.
- Shtokman, V.B. 1957. Influence of wind on the current in the Bering Strait, causes of their large velocity and predominantly northward direction (translated from the Russian by L.K. Coachman). *Trudy Institute of Oceanology, Akad. Nauk. SSSR, Moscow*, XXV, 171–197.
- Sigler, M.F., H.R. Harvey, J. Ashjian, M.W. Lomas, J.M. Napp, P.J. Stabeno, and T.I. Van Pelt. 2010. How does climate change affect the Bering Sea ecosystem? *Eos, Transactions, American Geophysical Union* 91(48):457–458, <http://dx.doi.org/10.1029/2010eo480001>.
- Stabeno, P.J., J.D. Shumacher, and K. Ohtani. 1999. The physical oceanography of the Bering Sea. Pp. 1–28 in *Dynamics of the Bering Sea: A Summary of Physical, Chemical, and Biological Characteristics, and a Synopsis of Research on the Bering Sea*. T.R. Loughlin and K. Ohtani, eds, North Pacific Marine Science Organization (PICES), University of Alaska Sea Grant, AK-SG-99-03.
- Steele, M., J. Morison, W. Ermold, I. Rigor, M. Ortmeyer, and K. Shimada. 2004. Circulation of summer Pacific halocline water in the Arctic Ocean. *Journal of Geophysical Research* 109, C02027, <http://dx.doi.org/10.1029/2003JC002009>.
- Stroeve, J., M.M. Holland, W. Meier, T. Scambos, and M. Serreze. 2007. Arctic sea ice decline: Faster than forecast. *Geophysical Research Letters* 34, L09501, <http://dx.doi.org/10.1029/2007GL029703>.
- Stroeve, J.C., T. Markus, L. Boisvert, J. Miller, and A. Barrett. 2014. Changes in Arctic melt season and implications for sea ice loss. *Geophysical Research Letters* 41:L216–L225, <http://dx.doi.org/10.1002/2013gl058951>.
- Torgerson, L.J., and W.J. Stringer. 1985. Observations of double arch formation in the Bering Strait. *Geophysical Research Letters* 12(10):677–680, <http://dx.doi.org/10.1029/GL012i010p00677>.
- Travers, C.S. 2012. *Quantifying Sea-Ice Volume Flux Using Moored Instrumentation in the Bering Strait*. University of Washington, MS thesis, 85 pp, http://psc.apl.washington.edu/HLD/Bstrait/TraversC2012_MScThesis_BeringStraitIceFlux.pdf.
- Tremblay, J.E., Y. Gratton, E.C. Carmack, C.D. Payne, and N.M. Price. 2002. Impact of the large-scale Arctic circulation and the North Water Polynya on nutrient inventories in Baffin Bay. *Journal of Geophysical Research* 107(C8), <http://dx.doi.org/10.1029/2000JC000595>.
- Vinje, T., N. Nordlund, and A. Kvambekk. 1998. Monitoring ice thickness in Fram Strait. *Journal of Geophysical Research* 103(C5):10,437–10,449, <http://dx.doi.org/10.1029/97JC03360>.
- Wadley, M.R., and G.R. Bigg. 2002. Impact of flow through the Canadian Archipelago and Bering Strait on the North Atlantic and Arctic circulation: An ocean modelling study. *Quarterly Journal of the Royal Meteorological Society* 128:2,187–2,203.
- Walsh, J.J., D.A. Dieterle, F.E. Muller-Karger, K. Aagaard, A.T. Roach, T.E. Whitledge, and D. Stockwell. 1997. CO₂ cycling in the coastal ocean: Part II. Seasonal organic loading of the Arctic Ocean from source waters in the Bering Sea. *Continental Shelf Research* 17:1–36, [http://dx.doi.org/10.1016/0278-4343\(96\)00021-0](http://dx.doi.org/10.1016/0278-4343(96)00021-0).
- Walsh, J.J., C.P. McRoy, L.K. Coachman, J.J. Goering, J.J. Nihoul, T.E. Whitledge, T.H. Blackburn, P.L. Parker, C.D. Wirick, P.G. Shuert, and others. 1989. Carbon and nitrogen cycling within the Bering/Chukchi Seas: Source regions for organic matter effecting AOU demands of the Arctic Ocean. *Progress in Oceanography* 22(4):277–259, [http://dx.doi.org/10.1016/0079-6611\(89\)90006-2](http://dx.doi.org/10.1016/0079-6611(89)90006-2).
- Weingartner, T.J., S. Danielson, Y. Sasaki, V. Pavlov, and M. Kulakov. 1999. The Siberian Coastal Current: A wind- and buoyancy-forced Arctic coastal current. *Journal of Geophysical Research* 104(C12):29,697–29,713, <http://dx.doi.org/10.1029/1999JC900161>.
- Weingartner, T., and T. Whitledge. 2013. The Pacific gateway to the Arctic: Quantifying and understanding Bering Strait oceanic fluxes. Pp. 19–23 in *Final Report on CIFAR's Shadow Award to NOAA on NA08OAR4320870, RUSALCA Russian-American Long-term Census of the Arctic, 1 July 2008–30 June 2013*. University of Alaska Fairbanks, http://www.cifar.uaf.edu/research/CIFAR_RUSALCA_NA08OAR4320870_final_report.pdf.
- Whitledge, T.E., and D.A. Stockwell. 2013. RUSALCA: Global change in the Arctic: Interactions of productivity and nutrient processes in the northern Bering and Chukchi Seas. Pp. 25–29 in *Final Report on CIFAR's Shadow Award to NOAA on NA08OAR4320870, RUSALCA Russian-American Long-term Census of the Arctic, 1 July 2008–30 June 2013*. University of Alaska Fairbanks, http://www.cifar.uaf.edu/research/CIFAR_RUSALCA_NA08OAR4320870_final_report.pdf.
- Woodgate, R.A. 2000. *Alpha Helix Cruise HX235 Bering Strait Cruise Report 2000*. 6 pp, <http://psc.apl.washington.edu/HLD/Bstrait/HX235cruisereport00.pdf>.
- Woodgate, R.A. 2001. *Alpha Helix Cruise HX250 Bering Strait Cruise Report 2001*. 12 pp, <http://psc.apl.washington.edu/HLD/Bstrait/HX250cruisereport01.pdf>.
- Woodgate, R.A. 2008. Mooring Cruise report for RUSALCA Sever cruise to the Bering Strait Aug/Sept 2007. University of Washington, 17 pp, <http://psc.apl.washington.edu/HLD/Bstrait/UWmooringreportSEVER2007Aug.pdf>.
- Woodgate, R. 2013. Arctic ocean circulation: Going around at the top of the world. *Nature Education Knowledge* 4(8):8.
- Woodgate, R.A., and K. Aagaard. 2005. Revising the Bering Strait freshwater flux into the Arctic Ocean. *Geophysical Research Letters* 32, L02602, <http://dx.doi.org/10.1029/2004GL021747>.
- Woodgate, R.A., K. Aagaard, and T.J. Weingartner. 2005a. Monthly temperature, salinity, and transport variability of the Bering Strait through-flow. *Geophysical Research Letters* 32, L04601, <http://dx.doi.org/10.1029/2004GL021880>.
- Woodgate, R.A., K. Aagaard, and T.J. Weingartner. 2005b. A year in the physical oceanography of the Chukchi Sea: Moored measurements from autumn 1990–1991. *Deep-Sea Research Part II* 52:3,116–3,149, <http://dx.doi.org/10.1016/j.dsr2.2005.10.016>.
- Woodgate, R.A., K. Aagaard, and T.J. Weingartner. 2006. Interannual changes in the Bering Strait fluxes of volume, heat and freshwater between 1991 and 2004. *Geophysical Research Letters* 33, L15609, <http://dx.doi.org/10.1029/2006GL026931>.
- Woodgate, R.A., K. Aagaard, and T.J. Weingartner. 2007. *First Steps in Calibrating the Bering Strait Throughflow: Preliminary Study of How Measurements at a Proposed Climate Site (A3) Compare to Measurements within the Two Channels of the Strait (A1 and A2)*. University of Washington, 20 pp, <http://psc.apl.washington.edu/HLD/Bstrait/A3asclimatesiteAug07.pdf>.
- Woodgate, R.A., and the Bering Strait 2013 Science Team. 2013. *Bering Strait Norseman II 2013 Mooring Cruise Report*. University of Washington, 59 pp, http://psc.apl.washington.edu/HLD/Bstrait/BeringStrait2013CruiseReport_Norseman2_3rdAug2013_wEL.pdf.
- Woodgate, R.A., S. Hartz, M. Kong, E. Ershova, V. Sergeeva, and K. Stafford. 2010a. *RUSALCA 2010: Bering Strait Mooring Cruise Report, July/August 2010*. University of Washington, http://psc.apl.washington.edu/HLD/Bstrait/CruiseReportKhromov2010wEL_verNov11.pdf.
- Woodgate, R.A., A. Nguyen, C. Peralta-Ferriz, R. Daniels, and J. Johnson. 2014. *Bering Strait Norseman II 2014 Mooring Cruise Report*. 73 pp., <http://psc.apl.washington.edu/HLD/Bstrait/NorsemanII2014Cruise.html>.
- Woodgate, R.A., and the RUSALCA 2011 Science Team. 2011. *RUSALCA: Bering Strait AON 2011 Mooring Cruise Report*. University of Washington, 58 pp., http://psc.apl.washington.edu/HLD/Bstrait/Khromov2011CruiseReportwithEL_Oct2011.pdf.
- Woodgate, R.A., and the RUSALCA 2012 Science Team. 2012. *RUSALCA: Bering Strait AON 2012 Mooring Cruise Report July 2012*. University of Washington, 77 pp., http://psc.apl.washington.edu/HLD/Bstrait/Khromov2012CruiseReport_vers6thFeb2015.pdf.
- Woodgate, R.A., T.J. Weingartner, and R.W. Lindsay. 2010b. The 2007 Bering Strait oceanic heat flux and anomalous Arctic sea-ice retreat. *Geophysical Research Letters* 37, L01602, <http://dx.doi.org/10.1029/2009GL041621>.
- Woodgate, R.A., T.J. Weingartner, and R. Lindsay. 2012. Observed increases in Bering Strait oceanic fluxes from the Pacific to the Arctic from 2001 to 2011 and their impacts on the Arctic Ocean water column. *Geophysical Research Letters* 39, L24603, <http://dx.doi.org/10.1029/2012gl054092>.
- Zhang, J.L., R. Woodgate, and S. Mangiameli. 2012. Towards seasonal prediction of the distribution and extent of cold bottom waters on the Bering Sea shelf. *Deep Sea Research Part II* 65–70:58–71, <http://dx.doi.org/10.1016/j.dsr2.2012.02.023>.

ACKNOWLEDGMENTS

Bering Strait physical oceanographic data are available via <http://psc.apl.washington.edu/BeringStrait.html> and the National Oceanographic Data Center (<https://www.nodc.noaa.gov>); ocean acidification data, via <http://aoncadis.org>; and marine mammal acoustic data, via <http://aoncadis.org> and <http://AOOS.org>. This article was funded by NOAA-RUSALCA and draws on logistics, data, and results from RUSALCA, NSF-ARC (0632154, 053026, 1107106, 1023264, and 1304052) and ONR (N00014-13-1-0468) projects. We thank K. Aagaard and T. Weingartner for scientific vision and championing of the Bering Strait moorings over the years; J. Johnson, D. Leech, and the scientists and crews of the vessels *Alpha Helix*, *CCGC Sir Wilfrid Laurier*, *Professor Khromov*, *Sever*, *Laurentiev*, and *Norseman2* for their dedicated work at sea; K. Runciman for data processing; NOAA/OAR/ESRL Physical Sciences Division, Boulder, CO, for the NOAA high-resolution SST data (<http://www.esrl.noaa.gov/psd>), and J. Raymond-Yakoubian and B. Fitzhugh for cultural insight.

AUTHORS

Rebecca A. Woodgate (woodgate@apl.washington.edu) is Senior Principal Oceanographer, Applied Physics Laboratory (APL), University of Washington (UW), Seattle, WA, USA. **Kathleen M. Stafford** is Principal Oceanographer, APL, UW, Seattle, WA, USA. **Fredrick G. Prah** is Professor Emeritus, College of Earth, Ocean and Atmospheric Sciences, Oregon State University, Corvallis, OR, USA.

ARTICLE CITATION

Woodgate, R.A., K.M. Stafford, and F.G. Prah. 2015. A synthesis of year-round interdisciplinary mooring measurements in the Bering Strait (1990–2014) and the RUSALCA years (2004–2011). *Oceanography* 28(3):46–67, <http://dx.doi.org/10.5670/oceanog.2015.57>.